# Statistical performance analysis of a fast super-resolution technique using noisy translations

Pierre Chainais, Aymeric Leray

# Statistical performance analysis of a fast super-resolution technique using noisy translations

Pierre Chainais, *Member, IEEE,* Aymeric Leray,

***Abstract*—The registration process is a key step for super-resolution (SR) reconstruction. More and more devices permit to overcome this bottleneck by using a controlled positioning system, e.g. sensor shifting using a piezoelectric stage. This makes possible to acquire multiple images of the same scene at different controlled positions. Then a fast SR algorithm [1] can be used for efficient SR reconstruction. In this case, the optimal use of $r^2$ images for a resolution enhancement factor $r$ is generally not enough to obtain satisfying results due to the random inaccuracy of the positioning system. Thus we propose to take several images around each reference position. We study the error produced by the SR algorithm due to spatial uncertainty as a function of the number of images per position. We obtain a lower bound on the number of images that is necessary to ensure a given error upper bound with probability higher than some desired confidence level. Such results give precious hints to the design of SR systems.**

***Index Terms*—high-resolution imaging; reconstruction algorithms ; super-resolution; performance evaluation ; error analysis**

## I. Introduction

SUPER-RESOLUTION (SR) will likely be implemented soon on every kind of camera from smartphones to DSLRs, compact system cameras or even microscopes and telescopes... This is made always easier thanks to many recent devices which facilitate multiframe acquisition and SR software. In particular, piezoelectric actuators which now achieve a positioning accuracy of fractions of nanometers [2] enable sensor shifting or moving platforms permitting to take several low-resolution (LR) pictures at slightly different globally translated positions. DSLR sellers (e.g. Ricoh/Pentax) recently announced new SR camera that will create high resolution (HR) images from sensor shift technology, as Hasselblad H5D-200MS and Olympus E-M5 Mark II are already doing. Numerous SR methods combining several low-resolution (LR) images to compute one high-resolution (HR) image have been developed, see [3] for a review. The registration step is often the bottleneck in terms of SR performance. Sensor shifting devices permit to reduce its impact thanks to the use of some controlled positioning system. To reach a given integer resolution enhancement factor $r$ (2, 3...), the optimal solution is to perform $r^2$ translations corresponding to displacements of $(k/r, \ell/r)$ in LR pixel units (1 LR pixel $= r$ HR pixels) for integers $(k, \ell) \in (0, r-1)^2$. The typical pixel size is of a few $\mu m$ nowadays.

Pierre Chainais is with Univ. Lille, CNRS, Centrale Lille, UMR 9189 - CRIStAL - Centre de Recherche en Informatique Signal et Automatique de Lille, F-59000 Lille, France. E-mail: pierre.chainais@ec-lille.fr. P. Chainais is grateful to Pierre Pfennig for helpful discussions.

Aymeric Leray is with ICB, CNRS UMR 6303, Université de Bourgogne, Dijon, France. E-mail: aymeric.leray@u-bourgogne.fr

However, the positioning system (or any registration method) only approximately reaches the targeted positions with some small random error. Based on a statistical performance analysis, we study the influence of this error on the quality of the SR images reconstructed with a simple and fast SR algorithm [1] which assumes that displacements are exactly known. We also study the importance of using several acquisitions of the same targeted positions to compensate for postioning errors in order to optimize the number of images required to ensure a given quality of the SR image. While the chosen SR method is *a priori* not as efficient as state of the art methods [4], the theoretical analysis of its statistical performance is possible, which would not likely be the case for other methods. Therefore, in addition to its rapidity, this method would come with theoretical guarantees on the quality of reconstruction. Moreover the adopted methodology paves the way to the analysis of more sophisticated SR methods, which is of great importance to give hints on the optimal co-conception of integrated SR imaging sytems.

Over the last 30 years, several works have dealt with mathematical analysis of SR algorithms, e.g. [5]–[13]. The works described in [5]–[7] essentially study the convergence of iterative methods for SR (e.g., conjugate gradient) including registration and deconvolution steps. They show that the reconstruction error decreases as the inverse of the number of LR images. In [8], the difficulty of the inverse problem is characterized by the conditioning number of a matrix defined from the direct model which is proportional to $r^2 s^2$ ($s =$ width of sensor pixels). When translations are uniformly distributed in $(0, r)^2$, this conditioning number tends to 1 and a direct inversion is possible with high probability when a large number of images is used [9]. In [10], the analysis was performed in the Fourier domain and showed that the mean square error decreases as the number of images increases when random translations are used. Ref. [11] quantifies the limitations of SR methods by computing Cramer-Rao lower bounds, also working in the Fourier domain. In the most favourable case where translations are known (no registration is needed), this bound is proportional to $r/n$ if $n$ is the number of images. All these works back to the 1980s [12] explain what makes SR difficult and how far more images can make it simpler. However, they have only expressed limited quantitative prediction beyond the qualitative $1/n$ behaviour of the reconstruction error. Our purpose is a detailed quantitative statistical error analysis of the simple Shift & Add method described in [1]. We obtain a lower bound on the number of images that is necessary to achieve a given error bound with high probability. The control of errors is crucial to produce nice looking results

but also to ensure reliable scientific observations. The present study is performed in the Fourier domain. The error at each frequency component is quantitatively evaluated. The use of Hoeffding's inequality permits to compute upper bounds and confidence intervals of practical use are obtained.

A preliminary work was presented at ICASSP 2014 in [14] with less general results because the assumptions were more restrictive (special uniform distribution). In this work, we use a more general and realistic assumption of bounded error on displacements. Furthermore, the potential presence of bias is taken into account and all mathematical proofs are given. The present results are tighter thanks to the use of Hoeffding's concentration inequality in place of the lose Bienaymé-Cebycev inequality. This article includes a numerical study and more detailed illustrations ; all useful Matlab codes are available.

Section II presents the setting and the model. Section III presents our main theoretical results which predict the required number of image acquisitions at each position to ensure some given confidence level in the reconstructed image. Sections III-A & III-B present the most technical aspects; proofs are in Appendix. Section III-C sums up our main theoretical results. Section IV presents numerical results. Section V discusses our contributions and some prospects.

## II. A FAST AND CONTROLLED SUPER-RESOLUTION TECHNIQUE

### A. The super-resolution problem

For a given SR factor $r$, the most common linear formulation of the general SR problem in the pixel domain is [1]:

$$Y_k \;=\; D_k H_k F_k Y_{HR} + n_k \qquad k = 1, .., K, \tag{1}$$

where $Y_{HR}$ is the (desired) high resolution image to estimate from the $K$ LR images $\{Y_k, 1 \leq k \leq K\}$. We assume the unknown HR image $Y_{HR}$ is a periodic bandlimited image sampled above the Nyquist rate. Each image $Y_k$ is a LR observation of the same underlying scene translated by $F_k$. The blur matrices $H_k$ model the point spread function (PSF) of the acquisition system and matrices $D_k$ are the decimation operator by a factor $r$. If $Y_{HR}$ is of size $r^2N^2 \times 1$ and $Y_k$ of size $N^2 \times 1$, matrices $F_k$ and $H_k$ are of size $(rN)^2 \times (rN)^2$ while $D_k$ are $N^2 \times (rN)^2$; $n_k$ is the noise, generally assumed to be Gaussian white noise so that $E(n_k n_k^t) = \sigma^2 I$. Images $Y_{HR}$, $Y_k$ and $n_k$ are rearranged in lexicographic ordered vectors. The least squares optimization problem can be formulated as:

$$\widehat{Y_{HR}} \;=\; \text{argmin}_Y \sum_{k=1}^{K} \|Y_k - D_k H_k F_k Y\|_2^2. \tag{2}$$

Other formulations based on the L1-norm or adding some regularization have also been proposed [15]. We focus on the method described in [1]: its simplicity makes it possible to quantitatively analyze its performances. Such a guarantee may be crucial for scientific imaging or the design of devices.

### B. Super-resolution algorithm

Several usual assumptions are used in [1]. The PSF of the acquisition system is known and spatially homogeneous so that $\forall k, H_k = H$. Decimation is the same for all images so that $\forall k, D_k = D$ in (1) & (2). We will also assume that the $r^2$ possible translated images at integer multiples $(k, \ell) \in (0, r-1)^2$ of the HR scale are available to provide an optimal setting for SR [11]. Then the solution to the least-square error SR problem (2) consists of two steps. A blurred image $Z = HY_{HR}$ can be estimated by [1]:

$$Z := HY_{HR} \;=\; \sum_{k=1}^{r^2} F_k^t D^t Y_k \tag{3}$$

The operation in (3) is equivalent to a simple interlacing of LR images, see Fig. 1. Then the final HR image results from the deconvolution of $Z$, which can be done using any algorithm such as Wiener or Lucy [16]. Such an approach separates the problem of SR into two steps of fusion (estimating $Z$) and deconvolution (deblurring to estimate $Y_{HR}$). This work focuses on the performance analysis of the fusion step only. Recall that high frequency terms at some $\mathbf{k}'$ are preserved if

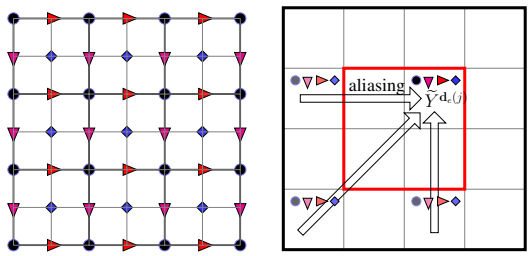


(a) (b)

Fig. 1. (a) Spatial domain: black disks and thick grid are the original LR sampling grid, the thin grid is the target HR grid. Other symbols are positions of 3 translated LR images of 1/2 LR pixel ($r = 2$); (b) Fourier domain: the inner (red) square contains LR frequencies $(-N/2, N/2)^2$, the outer square is for HR frequencies $(-rN/2, rN/2)^2$. Arrows represent aliasing, see (10).

| | |
|---|---|
| $r$ | super-resolution factor, typically $r = 2, 3...$ |
| $Y_{HR}$ | High Resolution (HR) image $\in \mathbb{R}^{(rN)^2}$ |
| $Y_k$ | Low Resolution (LR) image $\in \mathbb{R}^{N^2}$ |
| $n_k$ | noise in low resolution image $Y_k$ |
| $F_k$ | translation operator on HR images |
| $H_k$ | convolution blur operator on HR images |
| $D_k$ | decimation operator $N^2 \times (rN)^2$ |
| $\mathbf{d}$ | target position of one LR image |
| $Y^{\mathbf{d}}$ | HR image $Y$ translated by $\mathbf{d} = (d_x, d_y)$ |
| $\mathbf{b}_{\mathbf{d}j}$ | error on displacement $\mathbf{d}_e(j) = \mathbf{d} + \mathbf{b}_{\mathbf{d}j}$ |
| $n_{\mathbf{d}}$ | number of LR images around position $\mathbf{d}$ |
| $\epsilon$ | maximum positioning error in LR pixel units |
| $\eta$ | exponent of the spectrum of natural images |
| $\mathbf{k}$, $\mathbf{k}'$ | spatial frequency vectors resp. at LR and HR |
| $\widetilde{X}(\mathbf{k}') = [\mathcal{F}_{HR}X](\mathbf{k}')$ | Discrete Fourier Transform of HR image $X$ |
| $\widetilde{Y}(\mathbf{k}) = [\mathcal{F}_{LR}Y](\mathbf{k})$ | Discrete Fourier Transform of LR image $Y$ |
| $\mathcal{D}_{HR}$ | the set of spatial HR frequencies $\mathbf{k}'$ |
| $\mathcal{D}_{LR}$ | the set of spatial LR frequencies $\mathbf{k}$ |
| $\boldsymbol{\alpha}$, $\boldsymbol{\gamma}$ | vectors of 2D integer translations |
| $\mathbf{q}_{\boldsymbol{\alpha}}$, $\mathbf{q}_{\boldsymbol{\gamma}}$ | normalized frequencies |
| $p, p_1, p_2$ | relative absolute errors in $(0, 1)$ |
| $P_1, P_2$ | probabilities in $(0, 1)$ |
| $F^t$ | transpose of matrix $F$ |
| $\mathbb{E}[\,\cdot\,]$ | mathematical expectation |
| $\langle\,\cdot\,\rangle_{\mathbf{d}}$ | averging operator over $\mathbf{d}$ |

TABLE I
SUMMARY OF NOTATIONS.

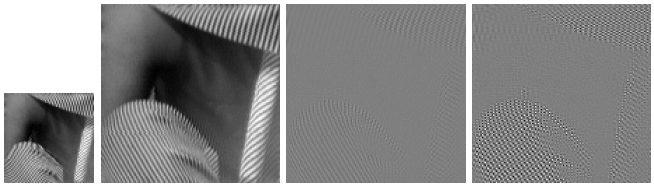

(a) (b) (c) (d)

Fig. 2. (a) Barbara, (b) Results from Algorithm [1] with $r = 2$, $\epsilon = 0.1$, $n_{\mathbf{d}} = 32$ im./pos. ; HF reconstruction error (zoom on screen), (c) $n_d = 32 \Rightarrow$ SNR$_{HF}$ =25.0dB, (d) $n_d = 1 \Rightarrow$ SNR$_{HF}$ =10.0dB.

and only if the PSF $\widetilde{H}(\mathbf{k}')$ is not zero. Some prior information might be used to reconstruct missing frequencies [11].

This algorithm requires one idealized assumption: displacements (matrices $F_k$) are assumed to be exact integer multiples of HR pixels. In practice, this is only approximately true due to the finite precision of the positioning system. Our purpose is to study the influence of this approximation. One solution would be to carry out accurate sub-pixel registration. This would remain insufficient since state of the art techniques cannot ensure a precision much better than 0.1-0.01 pixel [17], [18]. Another possibility is to take $n_{\mathbf{d}} \geq 1$ images for each required position so that the true $Z$ will be replaced by the estimate:

$$X = \hat{Z} = \sum_{\mathbf{d}} \frac{1}{n_{\mathbf{d}}} \sum_{j=1}^{n_{\mathbf{d}}} (F^{\mathbf{d}})^t D^t Y^{\mathbf{d}_e(j)} \tag{4}$$

$Y^{\mathbf{d}}$ is the image of a scene $Y$ translated by $\mathbf{d}$ where $\mathbf{d} = (d_x, d_y)$ denotes the targeted displacement vector; $\mathbf{d}_e(j) = \mathbf{d} + \mathbf{b}_{\mathbf{d}j}$ the real experimental displacement; $\mathbf{b}_{\mathbf{d}j}$ is the noise on the platform position. Note that in general $(F^{\mathbf{d}})^t F^{\mathbf{d}_e(j)} \neq I_{rN}$. One can hope to compensate from displacement inaccuracies by using multiple acquisitions at the same targeted position with some random error $\mathbf{b}_{\mathbf{d}j}$ around the expected value $\mathbf{d}$. A realistic assumption [2], [13], [19] is that the position error is bounded by $\epsilon > 0$ in LR pixel units or $\epsilon_r = \epsilon r$ in HR pixel units. For a given targeted position, the positioning system will be reset between each acquisition so that positions are randomly distributed around the average position (which may be biased due to miscalibration). This averaging process is expected to enhance the SR quality. Fig. 2 illustrates typical results from this approach applied to a detail of Barbara for $r = 2$, $\epsilon = 0.1$. The error on reconstructed high frequency components are compared for $n_{\mathbf{d}} = 1$ and $n_d = 32$ images/position. A SNR gain of about 15dB is observed when using 32 images (note for later use that $10\log_{10}(32) = 15$). Our aim is to reconstruct *probably approximately correct* (PAC) images by quantifying the number of images that should be taken per reference position to respect some given upper relative error bound of $p$ (e.g. 0.10) with probability (confidence) higher than $P$ (e.g. 0.90).

### C. Aliasing effects and notations

To detail the effect of aliasing, we consider the relation between the estimated blurred HR image $X$ defined by (4) and the LR images $Y^{\mathbf{d}_e(j)}$ in the Fourier domain, see Fig. 1(b). For some integer $n$, the interval $(-n : n)$ denotes the set of integers between $-n$ and $n$ (Matlab notations). When using the Discrete Fourier Transform (DFT), we denote by $\mathbf{k}$ the LR frequencies in $\mathcal{D}_{LR} = (-N/2 : N/2-1)^2$ and $\mathbf{k}'$ the HR frequencies in $\mathcal{D}_{HR} = (-rN/2 : rN/2-1)^2$. Given some HR frequency $\mathbf{k}'$, we need to deal with corresponding aliased terms in the LR image. The integer vector $\boldsymbol{\gamma} \in (-r : r)^2$ is such that $\mathbf{k} = \mathbf{k}' - \boldsymbol{\gamma} N \in \mathcal{D}_{LR}$. We denote by $\boldsymbol{\alpha}$ the integer vectors such that $\mathbf{k} + \boldsymbol{\alpha} N \in \mathcal{D}_{HR}$. Sums $\sum_{\mathbf{d}}$ are over all the $r^2$ ideal displacements $\mathbf{d} \in (0 : r-1)^2$ and sums over $\boldsymbol{\alpha}$ are sums over all possible HR frequencies $\mathbf{k}_{\boldsymbol{\alpha}} = \mathbf{k} + \boldsymbol{\alpha} N$ (up to $rN/2$). The DFT of image $Z$ is $\widetilde{Z}$. To alleviate formulas, we introduce the normalized frequencies:

$$\left\{ \begin{array}{rcl} \mathbf{q}_{\boldsymbol{\gamma}} & = & \frac{2\pi}{rN}\mathbf{k}' = \frac{2\pi}{rN}(\mathbf{k} + \boldsymbol{\gamma} N) = \mathbf{q} + \boldsymbol{\gamma}\frac{2\pi}{r} \\ \mathbf{q}_{\boldsymbol{\alpha}} & = & \frac{2\pi}{rN}(\mathbf{k} + \boldsymbol{\alpha} N) = \mathbf{q} + \boldsymbol{\alpha}\frac{2\pi}{r} \end{array} \right. \tag{5}$$

where $\boldsymbol{\alpha}, \boldsymbol{\gamma} \in \mathbb{Z}^2$. Note that $\mathbf{q}_{\boldsymbol{\alpha}} \in (-\pi, \pi)^2$ so that $\|\mathbf{q}_{\boldsymbol{\alpha}}\|_1 \leq 2\pi$ and $\|\mathbf{q}_{\boldsymbol{\alpha}}\|_2 \leq \sqrt{2}\pi$.

Back to (4), note that when $D$ is the decimation operator, $D^t$ is an upsampling operation (inserting zeros between samples) that produces aliasing. If $\mathcal{F}_{HR}$ is the HR DFT, for $\mathbf{k}' \in \mathcal{D}_{HR}$:

$$[\mathcal{F}_{HR} D^t Y^{\mathbf{d}_e(j)}](\mathbf{k}') = \widetilde{Y}^{\mathbf{d}_e(j)}(\mathbf{k} = \mathbf{k}' - \boldsymbol{\gamma} N) \tag{6}$$

Taking phase shifts due to translations of $(-\mathbf{d})$ associated to $(F^{\mathbf{d}})^t$ into account in the DFT of (4) yields:

$$\widetilde{X}(\mathbf{k}') = \sum_{\mathbf{d}} \frac{1}{n_{\mathbf{d}}} \sum_{j=1}^{n_{\mathbf{d}}} \widetilde{Y}^{\mathbf{d}_e(j)}(\mathbf{k}' - \boldsymbol{\gamma} N)\, e^{\frac{2i\pi}{rN}\mathbf{d}\cdot\mathbf{k}'} \tag{7}$$

Since each observation is a decimated version of the blurred translated scene, one has in the spatial domain:

$$Y^{\mathbf{d}_e(j)} = DHF^{\mathbf{d}_e(j)} Y_{HR} = DZ^{\mathbf{d}_e(j)} \tag{8}$$

In the Fourier domain:

$$\widetilde{Y}^{\mathbf{d}_e(j)}(\mathbf{k}) = [\mathcal{F}_{LR} D \mathcal{F}_{HR}^t \widetilde{Z}^{\mathbf{d}_e(j)}](\mathbf{k}) \tag{9}$$

and thanks to usual properties of the sum of roots of unity (see Appendix E):

$$\widetilde{Y}^{\mathbf{d}_e(j)}(\mathbf{k}) = \frac{1}{r^2} \sum_{\boldsymbol{\alpha}} \widetilde{Z}(\mathbf{k}_{\boldsymbol{\alpha}})\, e^{-\frac{2i\pi}{rN}\mathbf{k}_{\boldsymbol{\alpha}}\cdot\mathbf{d}_e(j)} \tag{10}$$

where we have used the fact that the homogeneous blur operator (convolution) is diagonal in Fourier domain. One can explicitly see in (10) how the information at high frequencies $\mathbf{k}_{\boldsymbol{\alpha}} = \mathbf{k} + \boldsymbol{\alpha} N$ from the HR image is aliased at low frequency $\mathbf{k}$ in each LR image $Y^{\mathbf{d}_e(j)}$. By separating the desired main contribution at $\mathbf{k}' = \mathbf{k} + \boldsymbol{\gamma} N$ and aliasing terms at $\mathbf{k} + \boldsymbol{\alpha} N$ for $\boldsymbol{\alpha} \neq \boldsymbol{\gamma}$, one gets by reporting (10) in (7):

$$\widetilde{X}(\mathbf{k}') = \widetilde{Z}(\mathbf{k}') G_{\boldsymbol{\gamma}}(\mathbf{k}') + B(\mathbf{k}') \tag{11}$$

$$B(\mathbf{k}') = \sum_{\boldsymbol{\alpha} \neq \boldsymbol{\gamma}} \widetilde{Z}(\mathbf{k} + \boldsymbol{\alpha} N) G_{\boldsymbol{\alpha}}(\mathbf{k}') \tag{12}$$

where

$$G_{\boldsymbol{\alpha}}(\mathbf{k}') = \frac{1}{r^2 n_{\mathbf{d}}} \sum_{\mathbf{d},j} e^{-i\frac{2\pi}{r}(\boldsymbol{\alpha}-\boldsymbol{\gamma})\mathbf{d}} e^{i\mathbf{q}_{\boldsymbol{\alpha}}\cdot\mathbf{b}_{\mathbf{d}j}} \tag{13}$$

(except when $k'_x$ or $k'_y$ is equal to $-rN/2$). In the ideal case where $\mathbf{b}_{\mathbf{d}j} = \mathbf{0}$ translations are exact multiples of HR pixels

and one retrieves $\widetilde{X} = \widetilde{Z} = \widetilde{H}\widetilde{Y}_{HR}$ since $G_{\boldsymbol{\gamma}} = 1$ and $G_{\boldsymbol{\alpha}} = 0$ for $\boldsymbol{\alpha} \neq \boldsymbol{\gamma}$. The first term in (11) is the *main approximation term*, which should be as close as possible to $\widetilde{Z}(\mathbf{k}')$. The second term $B(\mathbf{k}')$ in (11) is the *aliasing term* and should be as small as possible compared to the approximation term. Our purpose is to establish conditions for which $X$ is a good approximation of $Z$ within quantitative probabilistic bounds.

## III. Bounds on reconstruction errors

This section proves concentration inequalities that guarantee *PAC* SR. In this study, we make the general and realistic assumption that position errors are bounded so that $\mathbf{b}_{\mathbf{d}j} \in (-\epsilon_r, \epsilon_r)^2$ HR pixel units. We do not assume that $\mathbb{E}[\mathbf{b}_{\mathbf{d}j}] = 0$: the positioning system might be biased. In section III-A & III-B we deal with the coefficient $G_{\boldsymbol{\gamma}}$ of $Z$ in the main approximation term of (11) and then turn to the contribution of the aliasing term $B(\mathbf{k}')$. The reader interested in our main results only can directly move to sections III-C & III-D. Proofs are in Appendices B & C.

### A. Bound on the approximation term $G_{\boldsymbol{\gamma}}(\mathbf{k}')$

Since one expects that $\frac{1}{r^2}\mathbb{E}G_{\boldsymbol{\gamma}} \simeq 1$, we start from

$$\begin{aligned} |G_{\boldsymbol{\gamma}}(\mathbf{k}') - 1| \leq \\ |G_{\boldsymbol{\gamma}}(\mathbf{k}') - \mathbb{E}[G_{\boldsymbol{\gamma}}(\mathbf{k}')]| + |\mathbb{E}[G_{\boldsymbol{\gamma}}(\mathbf{k}')] - 1| \end{aligned} \tag{14}$$

Noting that $\mathbb{E}[G_{\boldsymbol{\gamma}}(\mathbf{k}')] = \mathbb{E}[e^{i\mathbf{q}_{\boldsymbol{\gamma}}\cdot\mathbf{b}_{\mathbf{d}j}}]$, the Taylor development of the complex exponential function yields[1]

$$\begin{aligned} \left|\mathbb{E}[e^{i\mathbf{q}_{\boldsymbol{\gamma}}\cdot\mathbf{b}_{\mathbf{d}_j}}] - 1\right| &\leq |\mathbf{q}_{\boldsymbol{\gamma}}.\mathbb{E}[\mathbf{b}_{\mathbf{d}j}]| + \mathbb{E}\left[\frac{(\mathbf{q}_{\boldsymbol{\gamma}}.\mathbf{b}_{\mathbf{d}_j})^2}{2}\right] \\ &\leq \underbrace{\|\mathbf{q}_{\boldsymbol{\gamma}}\|_2 \, \|\mathbb{E}[\mathbf{b}_{\mathbf{d}j}]\|_2 + \frac{\|\mathbf{q}_{\boldsymbol{\gamma}}\|_1^2 \, \epsilon_r^2}{2}}_{B_1} \end{aligned} \tag{15}$$

since $\mathbf{b}_{\mathbf{d}j} \in (-\epsilon_r, \epsilon_r)^2$. Then we deal with the first term in (14) by introducing:

$$B_G = \frac{1}{r^2 n_{\mathbf{d}}} \sum_{\mathbf{d},j} (e^{i\mathbf{q}_{\boldsymbol{\gamma}}\cdot\mathbf{b}_{\mathbf{d}_j}} - \mathbb{E}e^{i\mathbf{q}_{\boldsymbol{\gamma}}\cdot\mathbf{b}_{\mathbf{d}j}}) \tag{16}$$

To obtain concentration inequalities on $|B_G|$, our approach goes in 3 steps: i) bound the real and imaginary parts thanks to properties of their power series expansions, ii) prove concentration inequalities by using Hoeffding's inequality for the sum of differences between random variables and their expectations, iii) bound $|B_G|$ by using Lemma 1 below to combine bounds on the real and imaginary parts.

*Lemma 1:* (see proof in Appendix A) Let $x_1$ and $x_2$ two random variables in $\mathbb{R}$. Let $a_1, a_2 > 0$ and $P_1, P_2 \in (0,1)$ such that $P(|x_i| \geq a_i) \leq P_i$, $i = 1, 2$. Then

$$P(\sqrt{x_1^2 + x_2^2} \geq \sqrt{a_1^2 + a_2^2}) \leq P_1 + P_2 \tag{17}$$

$$P(|x_1| + |x_2| \geq a_1 + a_2) \leq P_1 + P_2 \tag{18}$$

Let us recall Hoeffding's inequality. *Hoeffding's inequality [21].* Let $\{X_i, 1 \leq i \leq n\}$ a set of independent random variables distributed over finite intervals $[a_i, b_i]$. Let $S = \sum_{i=1}^n (X_i - \mathbb{E}[X_i])$. For all $t > 0$,

$$P(|S| \geq t) \leq 2\exp\left(-\frac{2t^2}{\sum_{i=1}^n (b_i - a_i)^2}\right) \tag{19}$$

This permits to prove that, see Appendix B:

$$P\left(|B_G| \geq \underbrace{\sqrt{2}\left(\delta_{\boldsymbol{\gamma}} + \frac{\|\mathbf{q}_{\boldsymbol{\gamma}}\|_1^3 \epsilon_r^3}{3}\right)}_{B_2}\right) \leq 4e^{-c^2 n_{\mathbf{d}}/8} \tag{20}$$

We obtain the final concentration inequality for the main approximation term by combining (15) and (20) and going back to (14):

$$P\left(|G_{\boldsymbol{\gamma}}(\mathbf{k}') - 1| \geq B_1 + B_2\right) \leq 4e^{-c^2 n_{\mathbf{d}}/8} \tag{21}$$

for $\epsilon_r \leq 1/\pi r$, where $B_1$ and $B_2$ are defined in (15) & (20). Let $p \in (0,1)$ the maximum relative error constraint, e.g., $p = 0.1$, and $P_1 \in (0,1)$ such that $1 - P_1$ is the corresponding concentration probability. For sufficiently large $p$, one can define $\forall \mathbf{k}' \in \mathcal{D}_{HR}$ or $\mathbf{q}_{\boldsymbol{\gamma}} \in \frac{2\pi}{rN}\mathcal{D}_{HR}$ the adequate maximum coefficient $c(\mathbf{q}_{\boldsymbol{\gamma}}) > 0$ such that, neglecting the cubic term,

$$\sqrt{2}c(\mathbf{q}_{\boldsymbol{\gamma}})\|\mathbf{q}_{\boldsymbol{\gamma}}\|_1\epsilon + \|\mathbf{q}_{\boldsymbol{\gamma}}\|_2\langle\|\mathbb{E}[\mathbf{b}_{\mathbf{d},j}]\|_2\rangle_{\mathbf{d}} + \frac{\|\mathbf{q}_{\boldsymbol{\gamma}}\|_1^2\epsilon_r^2}{2} \leq p \tag{22}$$

$c(\mathbf{q}_{\boldsymbol{\gamma}})$ is a decreasing function of $\|\mathbf{q}_{\boldsymbol{\gamma}}\|_1$, which is minimum for maximal frequencies such that $\|\mathbf{q}_{\boldsymbol{\gamma}}\|_1 = 2\pi$. For $p$ large enough, one can define

$$\begin{aligned} c_1(p) &= \min_{\mathbf{q}_{\boldsymbol{\gamma}}} c(\mathbf{q}_{\boldsymbol{\gamma}}) = c(\pi, \pi) \\ &= \frac{1}{2\sqrt{2}\pi\epsilon}\left(p - \sqrt{2}\pi\langle\|\mathbb{E}[\mathbf{b}_{\mathbf{d},j}]\|_2\rangle_{\mathbf{d}} - 2\pi^2\epsilon^2 r^2\right) \end{aligned} \tag{23}$$

Then (22) with $c(\mathbf{q}_{\boldsymbol{\gamma}})$ replaced by $c_1(p)$ is true for all $\mathbf{q}_{\boldsymbol{\gamma}} \in \frac{2\pi}{rN}\mathcal{D}_{HR}$. When the averaged bias $\langle\mathbb{E}[e^{i\mathbf{q}_{\boldsymbol{\gamma}}\cdot\mathbf{b}_{\mathbf{d}_j}}]\rangle_{\mathbf{d}}$ is zero or remains negligible ($\ll p/\sqrt{2}\pi$),

$$c_1(p) \simeq \frac{p - 2\pi^2\epsilon^2 r^2}{2\sqrt{2}\pi\epsilon} \tag{24}$$

If $\epsilon \leq 1/\pi r$ and $c_1(p)$ is well defined, (21) becomes:

$$P\left(|G_{\boldsymbol{\gamma}}(\mathbf{k}') - 1| \geq p\right) \leq 4\exp\left(-\frac{c_1(p)^2 n_{\mathbf{d}}}{8}\right) \tag{25}$$

$\forall \mathbf{k}' \in \mathcal{D}_{HR}$. Then the relative error remains bounded by $p$ with probability larger than some $P_1 \in (0,1)$ if

$$n_{\mathbf{d}} \geq \frac{8}{c_1(p)^2}\log\left(\frac{4}{1 - P_1}\right) \tag{26}$$

The larger $c_1(p)$, the smaller the lower bound. This bound does not depend on the image content. In practice, it tells that, for $n_{\mathbf{d}}$ large enough, the main approximation term in (11) is less than $100p\%$ away from the targeted $\widetilde{Z}(\mathbf{k}')$ with probability larger than $P_1$. In ideal experimental conditions, with no bias and $\epsilon r \leq \sqrt{p/2\pi^2}$,

$$n_{\mathbf{d}} \geq \left(\frac{8\pi\epsilon}{p - 2\pi^2\epsilon^2 r^2}\right)^2 \log\left(\frac{4}{1 - P_1}\right) \tag{27}$$

[1] See Lemma 1 p. 512 in Feller (vol. 2) [20] on the Taylor development of $\exp(it)$ for $t > 0$.

For instance, see Tab. II, for $\epsilon = 0.01$, $r = 2$, $p = 0.1$ and $P_1 = 0.90$ (error $\leq 10\%$ with $\geq 90\%$ confidence level) this bound is $n_{\mathbf{d}} \geq 28$. The concentration level $(1 - P_1)$ can be very tight due to the logarithmic dependence of $n_{\mathbf{d}}$ on $(1 - P_1)$. At the same error level $p = 0.1$, the criterion becomes $n_{\mathbf{d}} \geq 45$ for $P_1 = 0.99$. In contrast, a much larger $n_{\mathbf{d}} \geq 5.3\,10^4$ is necessary to guarantee an accuracy of 1% ($p = 0.01$) at $P_1 = 0.90$ confidence level. In summary, confidence is cheap while accuracy is expensive. Note that the position accuracy $\epsilon$ should essentially decrease proportionally to $p$ as a finer reconstruction is desired. Moreover, given a desired SR factor $r$ and a position accuracy $\epsilon$, the relative error $p$ is lower bounded by $2\pi^2\epsilon^2 r^2$. For $r = 2$ and $\epsilon = 0.01$, the smallest relative error $p$ that can be guaranteed is $p_{best} = 0.008$.

### *B. Bound on the aliasing terms ($G_{\boldsymbol{\alpha}}, \boldsymbol{\alpha} \neq \boldsymbol{\gamma}$)*

The ideal situation in (11) occurs when the translations $\mathbf{d}$ are exactly the $r^2$ possible multiples of HR pixels. Due to properties of complex roots of unity, all the aliasing terms $G_{\boldsymbol{\alpha}}(\mathbf{k}')$ in (11) cancel for $\boldsymbol{\alpha} \neq \boldsymbol{\gamma}$. Our aim is to bound the contribution of aliasing error terms when translations are noisy due to approximate control only. The adopted strategy is similar to that of previous section, see proof in Appendix C. We also use the properties of roots of unity and a standard assumption on the spectral content of the target image. We start from (13):

$$G_{\boldsymbol{\alpha}}(\mathbf{k}') = \frac{1}{r^2 n_{\mathbf{d}}} \sum_{\mathbf{d},j} e^{-i\frac{2\pi}{r}(\boldsymbol{\alpha}-\boldsymbol{\gamma})\mathbf{d}} e^{i\mathbf{q}_{\boldsymbol{\alpha}}\cdot\mathbf{b}_{\mathbf{d}j}} \tag{28}$$

Let

$$\theta_{\boldsymbol{\alpha}\mathbf{d}} = \frac{2\pi}{r}(\boldsymbol{\alpha}-\boldsymbol{\gamma})\mathbf{d}, \quad \mathbf{d} \in (0:r-1)^2 \tag{29}$$

Note that the set of the $e^{i\theta_{\boldsymbol{\alpha}\mathbf{d}}}$ matches the set of products of complex roots of unity, see eq. (95)-(98) in Appendix E. The sum over translations $\sum_{\mathbf{d}}$ involves the sum of roots of unity, which is zero, in the computation of the aliasing term. In Appendix C, assuming that the variations of the bias $\mathbf{E}[\mathbf{q}_{\boldsymbol{\alpha}} \cdot \mathbf{b}_{\mathbf{d}j}]$ around $\langle \mathbf{E}[\mathbf{q}_{\boldsymbol{\alpha}} \cdot \mathbf{b}_{\mathbf{d}j}] \rangle_{\mathbf{d}}$ for fixed $\mathbf{d}$ are negligible, we prove the following concentration inequalities. For $\boldsymbol{\alpha} - \boldsymbol{\gamma} \notin \{0, r/2\}^2$ :

$$P\left(|G_{\boldsymbol{\alpha}}(\mathbf{k}')| \geq \sqrt{2}\delta'_{\boldsymbol{\alpha}}\right) \leq 4e^{-c^2 n_{\mathbf{d}}} \tag{30}$$

For $\boldsymbol{\alpha} - \boldsymbol{\gamma} \in \{0, r/2\}^2$, (79) in Appendix C gives a deterministic bound on the real part. Moreover $\sin(\theta_{\boldsymbol{\alpha}\mathbf{d}}) = 0$ in (80) so that one gets from (18) in Lemma 1:

$$P\left(|G_{\boldsymbol{\alpha}}(\mathbf{k}')| \geq \delta'_{\boldsymbol{\alpha}}\right) \leq 2e^{-c^2 n_{\mathbf{d}}} \tag{31}$$

which is even tighter than (30). In the special case $r = 2$, all $\boldsymbol{\alpha} - \boldsymbol{\gamma}$ are in $\{0, r/2\}^2 = \{0, 1\}^2$ so that we need (31) only and tighter bounds are obtained.

We aim at taking into account the contribution of all terms $\widetilde{Z}_{\boldsymbol{\alpha}} G_{\boldsymbol{\alpha}}(\mathbf{k}')$ for $\boldsymbol{\alpha} \neq \boldsymbol{\gamma}$ in (12). Let assume that they are independent. This is at least approximately true for two main reasons. First one can show that the $G_{\boldsymbol{\alpha}}(\mathbf{k}')$ are uncorrelated, see (111) in Appendix G and second the $\widetilde{Z}_{\boldsymbol{\alpha}}$ carry information about very distinct frequencies in the image. Then we can use Lemma 2 (see proof in Appendix A):

*Lemma 2:* Let $x_i$, $i = 1, ..., n$, $n$ independent random variables. Let $a_i > 0$ and $P_i \in (0, 1)$ $i = 1, ..., n$, such that $\forall i, P(|x_i| \geq a_i) \leq P_i$. Then

$$P\left(\sum_i |x_i| \leq \sum_i a_i\right) \geq \prod_{i=1}^{n}(1 - P_i) \tag{32}$$

Applying Lemma 2 to the set of $(r^2 - 1)$ possible $\boldsymbol{\alpha} \neq \boldsymbol{\gamma}$ from (30) yields a probabilistic bound on the relative aliasing error when $Z_{\boldsymbol{\gamma}} \neq 0$[2]:

$$P\left(\left|\sum_{\boldsymbol{\alpha}\neq\boldsymbol{\gamma}} \frac{\widetilde{Z}_{\boldsymbol{\alpha}}}{\widetilde{Z}_{\boldsymbol{\gamma}}} G_{\boldsymbol{\alpha}}(\mathbf{k}')\right| \leq \sqrt{2}\sum_{\boldsymbol{\alpha}\neq\boldsymbol{\gamma}} \left|\frac{\widetilde{Z}_{\boldsymbol{\alpha}}}{\widetilde{Z}_{\boldsymbol{\gamma}}}\right| \delta'_{\boldsymbol{\alpha}}\right) \geq \left(1 - 4e^{-c^2 n_{\mathbf{d}}}\right)^{r^2-1} \tag{33}$$

Given some desired relative error $p \in (0, 1)$ and lower probability $P_2 \in (0, 1)$, one needs to find whether there exists $c = c_2(p) > 0$ such that $\forall \mathbf{k}' \in \mathcal{D}_{HR}$

$$\sqrt{2}\sum_{\boldsymbol{\alpha}\neq\boldsymbol{\gamma}} \left|\frac{\widetilde{Z}_{\boldsymbol{\alpha}}}{\widetilde{Z}_{\boldsymbol{\gamma}}}\right| \underbrace{\left(c\|\mathbf{q}_{\boldsymbol{\alpha}}\|_1 \epsilon + f(\mathbf{q}_{\boldsymbol{\alpha}}, \epsilon_r)\right)}_{\delta'_{\boldsymbol{\alpha}}} \leq p, \tag{34}$$

A necessary condition appears as

$$p > p_0(\epsilon, r, Z) = \sqrt{2}\sum_{\boldsymbol{\alpha}\neq\boldsymbol{\gamma}} \left|\frac{\widetilde{Z}_{\boldsymbol{\alpha}}}{\widetilde{Z}_{\boldsymbol{\gamma}}}\right| f(\mathbf{q}_{\boldsymbol{\alpha}}, \epsilon_r) \tag{35}$$

Then one can define

$$c_2(p) = \inf_{\mathbf{q}_{\boldsymbol{\gamma}}} \sup_{c} \{c : \mathbf{q}_{\boldsymbol{\gamma}} \text{ obeys ineq.}(34)\} \tag{36}$$

If $c_2(p) > 0$ is well defined, then there exists a minimum number of images per position $n_{\mathbf{d}}$ such that

$$\left(1 - 4e^{-c_2(p)^2 n_{\mathbf{d}}}\right)^{r^2-1} \geq P_2, \tag{37}$$

that is

$$n_{\mathbf{d}}^{min} = \frac{1}{c_2(p)^2} \log\left(\frac{4}{1 - P_2^{\frac{1}{r^2-1}}}\right) \tag{38}$$

(39)

In the special case $r = 2$, (31) yields the even tighter bound:

$$n_{\mathbf{d}}^{min} = \frac{1}{c_2(\sqrt{2}p)^2} \log\left(\frac{2}{1 - P_2^{\frac{1}{3}}}\right). \tag{40}$$

One obtains a bound on the aliasing error relative to $|\widetilde{Z}(\mathbf{q}_{\boldsymbol{\gamma}})|$:

$$P\left(\left|\sum_{\boldsymbol{\alpha}\neq\boldsymbol{\gamma}} \frac{\widetilde{Z}_{\boldsymbol{\alpha}}}{\widetilde{Z}_{\boldsymbol{\gamma}}} G_{\boldsymbol{\alpha}}(\mathbf{k}')\right| \leq p\right) \geq P_2 \tag{41}$$

This relative error provides a good estimate of the relative error on the HR image before deconvolution. It permits to evaluate the contribution of aliasing errors to the reconstructed blurred HR image $Z$. This necessitates the knowledge of the true HR

[2]Note that one should first check that every term in the products are positive to ensure that the inequality above be relevant, which will be guaranteed by the final criterion.

image : one can also use the reconstructed image *a posteriori* to indicate which frequencies are most suspected to contribute to aliasing effects. Each specific image has a specific Fourier spectrum so that special aliasing effects may appear and make SR difficult, at least for a small set of frequencies for which the sum of aliasing terms in (41) may be particularly large. To propose a generic *a priori* estimate of the order of magnitude of this aliasing error, we need to make some assumptions on the content of images. It is well accepted that natural images often exhibit a power law energy spectrum $\propto 1/\|\mathbf{k}'\|_2^{2(1+\eta)}$ where usually $|\eta| \ll 1$ [22]–[24]. Then

$$\left|\frac{\widetilde{Z}_{\boldsymbol{\alpha}}}{\widetilde{Z}_{\boldsymbol{\gamma}}}\right| = \frac{|\widetilde{H}(\mathbf{q}_{\boldsymbol{\alpha}})|}{|\widetilde{H}(\mathbf{q}_{\boldsymbol{\gamma}})|}\left(\frac{\|\mathbf{q}_{\boldsymbol{\gamma}}\|_2}{\|\mathbf{q}_{\boldsymbol{\alpha}}\|_2}\right)^{1+\eta} \tag{42}$$

Therefore the strongest constraints are due to high frequencies (large $\mathbf{k}'$ or $\mathbf{q}_{\boldsymbol{\gamma}}$). Note the dependence on the blur kernel which acts as a low-pass filter: the presence of $\widetilde{H}$ in (42) will have adverse effects. Searching for lower-bounds, forthcoming computations consider the most favourable case when $\widetilde{H} = 1$. See section IV for a numerical illustration of the effect of a realistic Gaussian blur kernel. An approximate computation in App. D shows that the highest frequencies define $c_2^*(p)$ as

$$c_2^*(p) = \frac{p - p_0^*(\epsilon, r)}{a^*(\epsilon, H)} \tag{43}$$

where

$$\begin{aligned} p_0^*(\epsilon, r) &\simeq b_0\sqrt{2}^{\eta}\pi^2\epsilon^2 r^2(r^2-1) && (44)\\ a^*(\epsilon, H) &= \sqrt{2}\sum_{\boldsymbol{\alpha}\neq\boldsymbol{\gamma}}\frac{|\widetilde{H}(\mathbf{q}_{\boldsymbol{\alpha}})|}{|\widetilde{H}(\mathbf{q}_{\boldsymbol{\gamma}})|}\left(\frac{\|\mathbf{q}_{\boldsymbol{\gamma}}\|_2}{\|\mathbf{q}_{\boldsymbol{\alpha}}\|_2}\right)^{1+\eta}\|\mathbf{q}_{\boldsymbol{\alpha}}\|_1\epsilon \\ &\simeq a_0 2^{1+\eta/2}\epsilon(r^2-1) \quad (\text{if } \widetilde{H}=1) && (45)\end{aligned}$$

where the factor $(r^2-1)$ corresponds to the number of aliasing terms; the coefficient $b_0 \simeq 2/3$ for $r = 2$ and $b_0 \simeq 1.2$ for $r \geq 3$ and it is almost independent of the size $N$ of the image for $N \geq 32$; $a_0 \simeq 0.63$ for $r = 2$ and $a_0 \simeq 1.3$ for $r \geq 3$ (see Appendix D). In the general case, (44) & (45) interestingly permit to make explicit the dependence on $r$, $\epsilon$ and $\eta$. Thus, for a power-law spectrum image, the required minimum number $n_{\mathbf{d}}^{min}$ of images/position is:

$$n_{\mathbf{d}}^{min} = \frac{a^{*2}(\epsilon, H)}{(p - p_0^*(\epsilon, r))^2}\log\left(\frac{4}{1 - P_2^{\frac{1}{r^2-1}}}\right) \tag{46}$$

One observes that $p_0/\epsilon^2 r^2$ essentially depends on $r$ as soon as $\epsilon$ is small enough. Figure 3 illustrates numerical orders of magnitude of reachable $(p, \epsilon)$ such that $p > p_0^*(\epsilon, r)$ for given $r$ under the assumption of a power law spectrum. Pairs of acceptable parameters $(p, \epsilon)$ for which guaranteed error bounds exist are at the bottom right of each curve. Typical values can be evaluated numerically. For instance assuming $\eta = 0$, to guarantee an error smaller than 10%, $r = 2, p = 0.1 \Rightarrow \epsilon \leq 0.036$ or $r = 6, p = 0.1 \Rightarrow \epsilon \leq 0.0035$. Observe that $\epsilon$ should rapidly decrease as $r$ becomes larger when some given error level $p$ with high probability is desired. Note the logarithmic dependence on $(1 - P_2^{\frac{1}{r^2-1}})$ which permits to choose $P_2$ close to 1 without increasing $n_{\mathbf{d}}^{min}$ a lot.

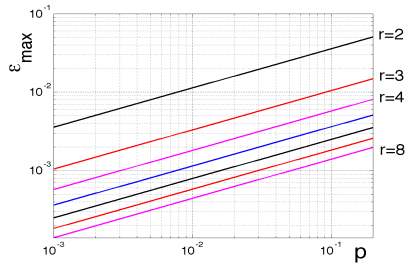


Fig. 3. Pairs of parameters $(p, \epsilon)$ for which SR with guaranteed error bounds is feasible are at the bottom right of the curve for each SR factor $r$ indicated on the right margin, see (44).

By using our results in the other way, one can also deduce a map of confidence intervals $p(\mathbf{q})$ for fixed $n_{\mathbf{d}}$. In practice, the acquisition protocole may impose some fixed $n_{\mathbf{d}}$. Then one can set the value of $c_2(p)$ in (34) and compute a map of confidence intervals $p(\mathbf{q})$ in the Fourier domain, taking into account the spectrum of the true HR image. Since it is not known, the Fourier transform may be replaced by its estimate. This procedure helps identifying which frequencies are more likely to contribute to aliasing errors.

### C. Main results

The analysis of the estimate $X$ of the blurred image $Z = HY_{HR}$ by the proposed algorithm gives in the spectral domain, see (11) & (12):

$$\begin{aligned} \widetilde{X}(\mathbf{k}') &= \widetilde{Z}(\mathbf{k}')G_{\boldsymbol{\gamma}}(\mathbf{k}') + B(\mathbf{k}') && (47)\\ B(\mathbf{k}') &= \sum_{\boldsymbol{\alpha}\neq\boldsymbol{\gamma}}\widetilde{Z}(\mathbf{k}+\boldsymbol{\alpha}N)G_{\boldsymbol{\alpha}}(\mathbf{k}') && (48)\end{aligned}$$

Theorem 3 below gathers the necessary assumptions on the acquisition system ($r$, $\epsilon$, $\mathbb{E}[\mathbf{b}_{\mathbf{d}j}]$), the scenes (spectrum exponent $\eta$ in (42)) and the desired confidence level ($p_1$ & $P_1$, $p_2$ & $P_2$) to obtain two fundamental concentration inequalities for the approximation and the aliasing terms respectively.

*Theorem 3:*

*Acquisition system* - Let $r$ be the SR factor. Let $0 < \epsilon < 1/\pi r$ be the maximum error of the positioning system (in LR pixel units). Assume bounded errors $\mathbf{b}_{\mathbf{d}j}$ on positions within $(-\epsilon r, \epsilon r)$ in both $x$ and $y$ directions with a possible constant bias $\mathbb{E}[\mathbf{b}_{\mathbf{d}j}]$ (in HR pixel units). Assume that $n_{\mathbf{d}}$ images are taken for each one of the $r$ necessary reference positions corresponding to $\mathbf{d} \in (0, r-1)^2$ HR pixel units.

*Confidence intervals* - Let $p_1 \in (0, 1)$, resp. $p_2 \in (0, 1)$ be the desired maximum relative error on the main approximation term, resp. the sum of aliasing terms, of the reconstructed image ($p_1$ & $p_2$ will generally be close to 0).

Let $P_1 \in (0, 1)$ be the desired level of confidence in the relative error $p_1$ due to the main approximation term. Let $P_2 \in (0, 1)$ be the level of confidence in the relative error $p_2$ due to the aliasing term ($P_1$ and $P_2$ will be close to 1).

*Technical assumptions* - Assume that one can define $c_1 > 0$ and $c_2 > 0$ by (dependences are omitted)

$$c_1 = \frac{1}{2\sqrt{2}\pi\epsilon}\left(p_1 - \sqrt{2}\pi\langle\|\mathbb{E}[\mathbf{b}_{\mathbf{d},j}]\|_2\rangle_{\mathbf{d}} - 2\pi^2\epsilon^2 r^2\right) \tag{49}$$

$$c_2(p_2) = \inf_{\mathbf{q_\gamma}} \sup_{c} \{c : L_{\boldsymbol{\gamma}}(c) \leq p_2\} \tag{50}$$

where function $f$ is defined by (77) and

$$L_{\boldsymbol{\gamma}}(c) = \sqrt{2} \sum_{\boldsymbol{\alpha} \neq \boldsymbol{\gamma}} \left| \frac{\widetilde{Z}_{\boldsymbol{\alpha}}}{\widetilde{Z}_{\boldsymbol{\gamma}}} \right| (c \|\mathbf{q}_{\boldsymbol{\alpha}}\|_1 \epsilon + f(\mathbf{q}_{\boldsymbol{\alpha}}, \epsilon_r)) \tag{51}$$

If

$$n_{\mathbf{d}} \geq \frac{8}{c_1(p_1)^2} \log\left(\frac{4}{1-P_1}\right) \tag{52}$$

then the following probabilistic inequality holds:

$$P\left(\left\{\forall \mathbf{k}' \in \mathcal{D}_{\mathcal{HR}}, \left|\frac{G_{\boldsymbol{\gamma}}(\mathbf{k}', n_{\mathbf{d}})}{r^2} - 1\right| \leq p_1\right\}\right) \geq P_1 \tag{53}$$

If

$$n_{\mathbf{d}} \geq \begin{cases} \dfrac{1}{c_2(\sqrt{2}p)^2} \log\left(\dfrac{2}{1-P_2^{\frac{1}{3}}}\right) & \text{if } r = 2, \\ \dfrac{1}{c_2(p)^2} \log\left(\dfrac{4}{1-P_2^{\frac{1}{r^2-1}}}\right) & \text{if } r \geq 3. \end{cases} \tag{54}$$

then the following concentration inequality holds:

$$P\left(\left\{\forall \mathbf{k}' \in \mathcal{D}_{\mathcal{HR}}, \left|\frac{B(\mathbf{k}', n_{\mathbf{d}})}{\widetilde{Z}(\mathbf{k}')}\right| \leq p_2\right\}\right) \geq P_2 \tag{55}$$

*Let us comment on Theorem 3.* In ideal experimental conditions, with no positioning bias and $\epsilon r \leq \sqrt{p/2\pi^2}$,

$$c_1(p) \simeq \frac{p - 2\pi^2\epsilon^2 r^2}{2\sqrt{2}\pi\epsilon} \tag{56}$$

The quantity $c_2(p_2)$ can be computed numerically for some given specific image. A necessary condition to the existence of $c_2(p_2)$ is

$$p_2 > p_0(\epsilon, r, Z) = \sqrt{2} \sup_{\mathbf{q_\gamma}} \sum_{\boldsymbol{\alpha} \neq \boldsymbol{\gamma}} \left| \frac{\widetilde{Z}_{\boldsymbol{\alpha}}}{\widetilde{Z}_{\boldsymbol{\gamma}}} \right| f(\mathbf{q}_{\boldsymbol{\alpha}}, \epsilon_r) \tag{57}$$

In the most favourable case when $\widetilde{H} = 1$ (no blur) and the image has a power law Fourier spectrum $\propto \|\mathbf{k}'\|_2^{-2(1+\eta)}$, (44) permits to estimate $p_0(\epsilon, r, Z)$. Then $c_2(p_2)$ can be computed from (43) which is easy to use and gives quantitative indications about $n_{\mathbf{d}}$.

*Corollary 4:* Under the assumptions of Theorem 3 and denoting $c_1 = c_1(p_1)$ and $c_2 = c_2(p_2)$, if a sufficient number $n_{\mathbf{d}}$ of images per position is used, one has the following concentration inequality which guarantees a small relative error with high probability:

$$\begin{aligned} P\left(\left\{\forall \mathbf{k}' \in \mathcal{D}_{\mathcal{HR}}, \left|\frac{\widetilde{X}(\mathbf{k}') - \widetilde{Z}(\mathbf{k}')}{\widetilde{Z}(\mathbf{k}')}\right| \leq p_1 + p_2\right\}\right) \\ \geq P_2 - (1 - P_1) \\ \geq \left(1 - 4e^{-c_2^2 n_{\mathbf{d}}}\right)^{r^2-1} - 4e^{-\frac{c_1^2 n_{\mathbf{d}}}{8}} \end{aligned} \tag{58}$$

*Proof :* this is a direct consequence of Lemma 1 p. 4 applied to the sum of the approximation term $|G_\gamma/r^2 - 1|$ and the aliasing term $|B/\widetilde{Z}|$.

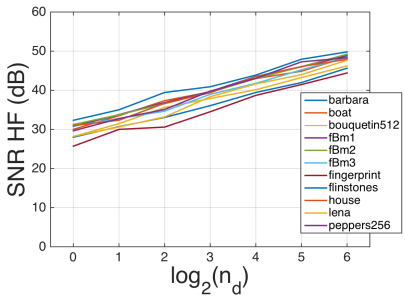


Fig. 4. SNR for high frequencies only is proportional to $\log_{10} n_{\mathbf{d}}$. Results from 100 Monte-Carlo simulations with uniform distribution of positions with $\epsilon = 0.01$ for 11 images (Lena, Barbara, Boat...).

Corollary 4 gives a probabilistic bound to the total relative error on each frequency component of the reconstructed blurred image $Z$ using the algorithm from [1] before the deconvolution step. Note that the bound in probability in (58) tends to 1 exponentially fast when $n_{\mathbf{d}} \to \infty$. In practice, one can guarantee a global relative error $\leq 10\%$ with probability $\geq 0.90$ by choosing $(p_i, P_i) = (0.05, 0.95)$, i=1,2. This result provides a precise quantitative analysis of the reconstruction error. One limitation of the present study is that $\widetilde{Z}(\mathbf{k}') = H(\mathbf{k}')Y_{HR}(\mathbf{k}')$ is the blurred super-resolved image resulting from the fusion of LR images. However the deconvolution step is common to every acquisition system and remains a limitation of any SR approach. Of course, the most favourable situation is when $H(\mathbf{k}')$ is close to 1, corresponding to a Dirac PSF in the spatial domain. Then Corollary 4 gives a good indication of the quality of high resolution imaging by using multiple acquisitions per positions.

In summary, we propose a detailed analysis of the reconstruction error of a fast method in the Fourier domain. It provides an a priori estimate of the number of images/position necessary to guarantee a given quality of reconstruction of each frequency (Fourier mode) with high probability. Based on Monte Carlo simulations, it also allows to estimate a posteriori a map of confidence levels in the frequency domain. Section IV will show numerically that these bounds are tight. We have worked on the intermediate reconstructed image $Z$ before the deconvolution step that is common to most SR methods. Theorem 3 can be used based on the generic assumption of a power-law spectrum that is usual for natural images or more specifically for one specific image.

### D. What about the SNR ?

We have demonstrated theoretical bounds to control the quality of the super resolved image in the Fourier domain. However this result deals with each frequency separately. Now we aim at identifying the dependence of the SNR between the reconstructed image and the ground truth. Again, this SNR deals with $Z$ not $Y_{HR}$ and it measures the quality of the fusion step and does not consider the posterior deconvolution effects.

We consider the mean square error :

$$\left\|\widetilde{X}-\widetilde{Z}\right\|_2^2=\sum_k \underbrace{\left|\frac{\widetilde{X}(\mathbf{k}')-\widetilde{Z}(\mathbf{k}')}{\widetilde{Z}(\mathbf{k}')}\right|^2}_{\alpha^2_{\mathbf{k}'}}\cdot|\widetilde{Z}(\mathbf{k}')|^2 \tag{59}$$

and compare it to the energy of the original HR image. The $|\widetilde{Z}(\mathbf{k}')|$ are considered as fixed (the ground truth) while the $\alpha_{\mathbf{k}'}$ are random variables here (relative error estimates). Now we show that $\mathbb{E}\alpha^2_{\mathbf{k}'}$ is of the order of $1/n_{\mathbf{d}}$ for all $\mathbf{k}'$ so that $SNR\propto\log n_{\mathbf{d}}$. From (58) in Corollary 4,

$$P(|\alpha_{\mathbf{k}'}|\leq p)\geq 1-4r^2e^{-c^2n_{\mathbf{d}}} \tag{60}$$

where $c^2(p)=\min(c_2^2(p),c_1^2(p)/8)$. Note from (43) & (56) that the typical order of magnitude of $c_1(p)$ and $c_2(p)$ is $p/\epsilon$ so that we can consider that there exists $\lambda>0$ such that $c^2\geq\lambda p^2/\epsilon^2$. Then

$$\begin{aligned}\mathbb{E}[\alpha^2_{\mathbf{k}'}] &\leq \int_{|\alpha_{\mathbf{k}'}|\leq p}\alpha^2_{\mathbf{k}'}p(\alpha_{\mathbf{k}'})d\alpha_{\mathbf{k}'}+\int_{|\alpha_{\mathbf{k}'}|\geq p}\alpha^2_{\mathbf{k}'}p(\alpha_{\mathbf{k}'})d\alpha_{\mathbf{k}'}\\ &\leq p^2+2\sum_{n=1}^{\infty}\int_{np}^{(n+1)p}\alpha^2_{\mathbf{k}'}p(\alpha_{\mathbf{k}'})d\alpha_{\mathbf{k}'}\\ &\leq p^2+4r^2\sum_{n=1}^{\infty}e^{-\lambda n^2p^2n_{\mathbf{d}}/\epsilon^2}(n+1)^2p^2\\ &\leq p^2(1+e^{-\lambda p^2n_{\mathbf{d}}/\epsilon^2}K(n_{\mathbf{d}}))\end{aligned} \tag{61}$$

where $K(n_{\mathbf{d}})$ is finite, decreasing with $n_{\mathbf{d}}$ and independent of $\mathbf{k}'$. Choosing $p^2=1/n_{\mathbf{d}}$, one obtains for all $\mathbf{k}'\in\mathcal{D}_{HR}$,

$$\mathbb{E}[\alpha^2_{\mathbf{k}'}]\leq\frac{1}{n_{\mathbf{d}}}(1+e^{-\lambda/\epsilon^2}K(n_{\mathbf{d}})) \tag{62}$$

and consequently taking the expectation of (59),

$$\begin{aligned}\mathbb{E}\left[\left\|\widetilde{X}-\widetilde{Z}\right\|_2^2\right]&=\sum_{\mathbf{k}'}\mathbb{E}[\alpha^2_{\mathbf{k}'}]|\widetilde{Z}(\mathbf{k}')|^2\\ &\leq\frac{1}{n_{\mathbf{d}}}(1+e^{-\lambda/\epsilon^2}K(n_{\mathbf{d}}))\|\widetilde{Z}\|_2^2\end{aligned} \tag{63}$$

Finally, using Parceval's equality we get:

$$\mathrm{SNR}(\widetilde{X},\widetilde{Z})\geq 10\log_{10}n_{\mathbf{d}}+K \tag{64}$$

where $K$ is a constant depending on the energy of the original image. As a function of the number of images per position $n_{\mathbf{d}}$, the SNR is improved with a magnitude of 10dB/decade. We can compare this result with the weak Cramer-Rao lower bound on the reconstruction error $T_{weak}\propto 1/\sqrt{K+1}$ where $K+1$ is the number of images in [11] : at best, the SNR can grow as log(number of images) as predicted by (64). This indicates that the proposed method is efficient at the best expected level [5]–[12]. Fig. 4 shows SNR computed for high frequencies only (the reconstructed HR part of the spectrum). Results were computed from 100 Monte-Carlo simulations with uniform distribution of position errors with $\epsilon=0.01$ for 11 images (Lena, Barbara, Boat...). This global indication that the SNR is $\propto\log n_{\mathbf{d}}$ completes previous detailed bounds for each Fourier component.

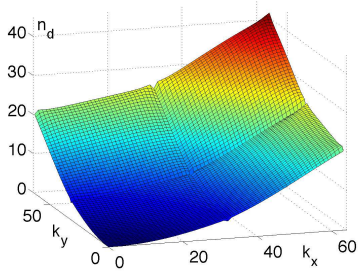


Fig. 5. Minimum number $n_{\mathbf{d}}(\mathbf{k}')$ to guarantee an aliasing error $\leq 5\%$ with probability $\geq 0.95$ for all $\mathbf{k}'$ ; $\epsilon=0.001$, $r=4$.

## IV. Numerical results

To illuminate the complex interplay between the many parameters involved, we study the problem from various viewpoints. Section IV-A studies the lower-bound on the number $n_{\mathbf{d}}$ of images per position to guarantee a given maximum errror level. Section IV-B compares our theoretical results to numerical estimates of probabilities from Monte-Carlo simulations. Section IV-C studies the connection between results in the Fourier domain and in the spatial domain. Section IV-D shows how the presence of noise and the nature of the blur operator influence the results. Monte-Carlo simulations use 100 realizations of the acquisition procedure assuming a uniform distribution of position errors in $(-\epsilon,\epsilon)$. When no image is specified, the power law spectrum assumption is used.

### *A. How many images to ensure some maximum error level ?*

Fig. 5 shows the dependence of the required number of images $n_{\mathbf{d}}(\mathbf{k}')$ on the frequency $\mathbf{k}'$ to guarantee that aliasing contribution is less than $p_1=0.05$ with probability $P_1\geq 0.95$ when $r=4$ and $\epsilon=0.001$ for an image with a power law spectrum. As expected, the recovery of high frequencies requires more LR images. The results are nearly independent of the size $N$ of images for $N\geq 32$. A similar picture (not shown) stands for the approximation term. In general (not always) the control of aliasing effects is the most constraining.

Tab. II gathers the constraints for various values of $r$ and $\epsilon$ for images with a power law spectrum ($\eta=0$ here). Numbers are computed from (52) & (54) in Theorem 3 for parameters $(p_i,P_i)$ = (0.05,0.95), $i=1,2$. This choice of equidistribution of error is certainly not optimal but of practical use with respect to Corollay 4 garantying an error level $\leq p_1+p_2=0.10$ with probability larger than $P_2-(1-P_1)=0.90$. The larger $r$, the larger the need for multiple images. The smaller the positioning uncertainty $\epsilon$, the smaller the lower bound on $n_{\mathbf{d}}$.

As an example, we consider a setting where the sensor has LR pixels of width $\simeq 1\ \mu m$. The random bias on the positioning system can be reasonably expected to be between 1 and 10 nm corresponding to $\epsilon\simeq 0.001-0.01$ LR pixel. The acquition rate of images is usually of the order of 10 im./s (e.g. in a DSLR). In practice, $r^2$ displacements are used so that a minimum acquisition time of about $r^2\times n_{\mathbf{d}}\times 0.1$s is necessary. For $r=2$ and $\epsilon=0.01$, relative errors $\leq 5\%$ on the restored image can be guaranteed with probability $\geq 0.95$

| images with a power law spectrum | | | |
|---|---|---|---|
| $\epsilon$ | 0.01 | 0.001 | 0.0001 |
| | approx. / alias | app. / alias | app. / alias |
| $r=2$ | 157 / 64 | 2 / 1 | 1 / 1 |
| PSF(0.5) | 157 / 6108 | 2 / 23 | 1 / 1 |
| $r=3$ | 267 / NR | 2 / 13 | 1 / 1 |
| PSF(0.5) | 267 / NR | 2 / 540 | 1 / 5 |
| $r=4$ | 817 / NR | 2 / 43 | 1 / 1 |
| PSF(0.5) | 817 / NR | 2 / 2228 | 1 / 13 |
| $r=5$ | 651162 / NR | 2 / 168 | 1 / 2 |
| PSF(0.5) | 651162 / NR | 2 / 73025 | 1 / 43 |
| $r=6$ | NR / NR | 2 / 516 | 1 / 3 |
| PSF(0.5) | / NR | 2 / NR | 1 / 82 |
| $r=7$ | NR / NR | 2 / 3486 | 1 / 6 |
| PSF(0.5) | / NR | 2 / NR | 1 / 189 |
| $r=8$ | NR / NR | 2 / NR | 1 / 9 |
| PSF(0.5) | / NR | 2 / NR | 1 / 311 |

TABLE II

MINIMUM $n_{\mathbf{d}}$ FOR ACCURACY $< 5\%$ WITH PROBABILITY $> 0.95$ ON APPROX./ALIASING AS A FUNCTION OF $\epsilon$ IN LR PIXEL UNITS. PSF(0.5) IS GAUSSIAN BLUR OF WIDTH 0.5; NR='NOT REACHABLE' (SEE TEXT).

by using at least $n_{\mathbf{d}} = 157$ (approximation), resp. $n_{\mathbf{d}} = 64$ (aliasing) images/position. Taking into account both contributions (approximation + aliasing) implies $n_{\mathbf{d}} \geq \max(157, 64)$ so that $n_{\mathbf{d}} = 157$ im./pos. are necessary. The acquisition time would be $r^2 \times 157 \times 0.1s = 63$s. With a position accuracy of $\epsilon = 0.01$ only, the potential for SR of the proposed technique remains very limited : for $r = 3$ there is no way to guarantee a quality of reconstruction with an aliasing error less than $5\%$ (NR = "Not Reachable" in Tab. II). When $\epsilon = 0.001$ the acquisition of $r^2 \times 13 = 117$ images ($\simeq$ 12s at 10 im./s) permits to guarantee a relative error $\leq 10\%$ with probability $\geq 0.90$. For $r = 4$, more than 43 im./pos. are necessary which leads to an acquisition time of about 69s that is reasonable for still scenes. For $r = 6$, $r^2 \times 516 = 18576$ images would take $\simeq$ 30 min at 10 im./s which becomes technically difficult, even regardless of other physical limitations of the system. One also observes that a registration accuracy of $10^{-4}$ LR pixels would be sufficient to ensure good SR conditions even for large SR factors. Remember that these predictions on $n_{\mathbf{d}}$ are based on the generic assumption of a power law spectrum which is statistically common to many natural images. In full rigor, even though these numbers are of great use in practice to calibrate the acquisition system, they should be estimated for each image individually: then the full map of the bounds in the Fourier domain can be computed.

For comparison, [13] showed that only a special set of vertices is really useful to SR; more images at other positions will bring marginal supplemental information. However the uncertainty on registration was not considered. No noise was introduced in synthetic experiments, and the registration was assumed exact. In real experiments, the uncertainty on positions was about 0.1 LR pixel: the authors observed no improvement when using more and more images. The present study confirms this conclusion and shows that a 0.1 pixel registration accuracy is not sufficient to expect any significant improvement by using more LR images, see tab. II. Misregistration should remain typically smaller than 0.01 LR pixel.

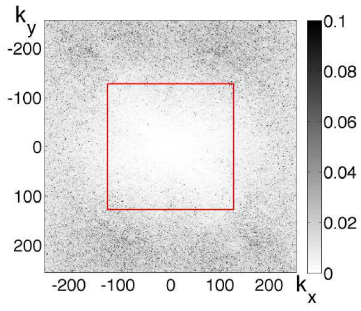


Fig. 6. Fourier map of the lower bound on the aliasing error $p_2$ within $(0, 0.1)$ for Lena. The red square indicates LR frequencies. $r = 2$ & $\epsilon = 0.01$: for black points (0.9% points are $> 0.1$), SR with guaranteed error bound is not feasible (100 MC simulations).

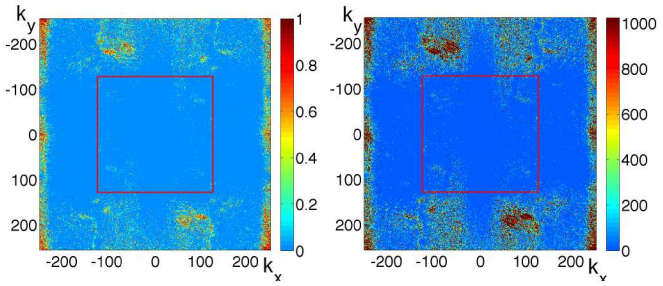


Fig. 7. In Fourier domain, for image Barbara, $r = 2$ and $\epsilon = 0.01$: (left) probability that relative error due to aliasing be $\geq 0.1$ using $n_{\mathbf{d}} = 64$ im/pos. ; (right) minimum number of images to ensure an aliasing error $< 10\%$.

### *B. How realistic and tight are these bounds ?*

The bounds from Theorem 3 can first be considered to dimension the acquisition system. They can also be used to check the reliability or accuracy of some specific restored image. Using (57) we can compute a map of the lower bound on the aliasing error $p_2$ in the HR Fourier domain given the motion accuracy $\epsilon$: this map shows the best achievable relative accuracy for each frequency $\mathbf{k}'$. For Lena, $r = 2$, $\epsilon = 0.01$, fig. 6 shows the map computed from 100 Monte-Carlo simulations over uniformly distributed positioning errors in $(-\epsilon, \epsilon)$. Gray points are such that a sufficient number of images/position should guarantee a relative error $< 10\%$ with high probability. Few black points where the lower bound of $p_2$ is $> 0.1$ correspond to spatial frequencies for which an error $< 10\%$ cannot be guaranteed, whatever the number $n_{\mathbf{d}}$ of images/position mainly because of excessive aliasing. As expected, we observe that high frequencies are the most difficult to reconstruct accurately. Fig. 7(left) shows in Fourier domain the probability that the aliasing error at $\mathbf{k}'$ be $\geq 10\%$ when using 32 im./position for Barbara with $\epsilon = 0.01$ and $r = 2$. Fig. 7(right) shows the number $n_{\mathbf{d}}$ of images necessary to ensure that aliasing error $\leq 10\%$ according to Theorem 3. Note the consistency between these pictures. Aliasing effects are a direct consequence of the image spectrum: some frequencies are much more difficult to reconstruct and call for a larger $n_{\mathbf{d}}$.

### C. How are the errors localized in the spatial domain ?

We use Monte-Carlo simulations to study the localization of errors in the *spatial domain*. By selecting the less reliable frequency components of an image where the aliasing error is $\geq 10\%$ with probability $\geq 0.1$, one can reconstruct the corresponding spatial counterpart to localize and quantify their contribution. For $r = 2$, $\epsilon = 0.01$, these unreliable components weight for a SNR of -27.2dB. The present theoretical analysis permits such a selection of frequencies as well. For a given number $n_{\mathbf{d}}$ of images/position one can reconstruct the spatial counterpart of the less reliable frequencies where the aliasing error is expected to be $\geq 10\%$ with probability $\geq 0.1$ according to Theorem 3. Fig. 8 shows such a picture for *Barbara* for $r = 2$, $\epsilon = 0.01$ and $n_{\mathbf{d}} = 256$ im./pos., to be compared with the minimum $n_{\mathbf{d}} = 157$ in Tab. II. As expected, the spoiled regions are the most textured ones as well as some contours (better seen on screen). Remember that the analysis focused on the modulus of Fourier spectra while phases carry the location information. Maximum gray levels are about 4 and the standard deviation is of 0.67 (to compare with 255 in 8 bits). These "non reliable" components then weight for a SNR of -25.8 dB w.r.t. superresolved frequencies only. At least on this example, our theoretical predictions both qualitatively and quantitatively agree with Monte Carlo results. Our analysis not only gives indications to choose $n_{\mathbf{d}}$ but also produces a detailed map of the error distribution both in the Fourier domain and in the spatial domain.

### D. How do noise and PSF influence performances ?

The influence of noise and PSF are two important questions. The problem of noise is not the most critical: averaging numerous images attenuates additive noise. The present approach considers additive contributions of numerous images affected by independent realizations of noise: this naturally tends to increase the SNR. This is easily checked experimentally and not illustrated here for sake of briefness. If the noise in LR images was too strong to be compensated by simple averaging, the utility of SR would be questionable since the main concern would first be to access reliably denoised information at low resolution, giving up hopes for high resolution. Here we assume that LR images are of sufficient quality. The question of the PSF is a much bigger concern since it is involved in the error analysis. Of course frequencies where $\widetilde{H}(\mathbf{k}') = 0$ are lost and we already mentionned that the present analysis is not valid for these frequencies. Moreover the structure of aliasing is influenced by the PSF in an important manner, see (42). All the experiments above considered the ideal situation of a Dirac PSF where $\widetilde{H}(\mathbf{k}') = 1\ \forall \mathbf{k}'$. The lines 'PSF(0.5)' in Tab. II show how the lower bounds of $n_{\mathbf{d}}$ are modified in presence of a Gaussian PSF of width 0.5. As expected it dramatically influences the estimates, e.g. for $(r, \epsilon) = (2, 0.001)$ as the bound becomes 18 in place of 1. The control of the PSF is a real stake in the design of a SR system: the present study permits to quantitatively evaluate its influence.

## V. Conclusion

We have presented a theoretical analysis of a cheap and fast SR technique which takes benefit from any accurate controlled positioning system, e.g. piezoelectric actuators for sensor shifting, now currently available on many optical systems. Such an approach comes with some constraints. It requires a static scene captured using a static camera in good lighting conditions to avoid a high level of noise. It may also suffer from a lack of depth of field or an inhomogeneity of translations between images due to parallax for instance. However the statistical analysis of the algorithm proposed in [1] produces error confidence intervals as a function of the number of available images. This is made possible by the simplicity of the algorithm itself and by exploiting the averaging effect of LR images taken at positions that are randomly distributed around the same reference position. This approach is cheap and realistic to enhance the resolution of many devices. Even not state of the art, theoretical guarantees are a strong advantage of the approach when the reliability of the restored image is at stake, e.g. in scientific imaging (biology, astronomy...). This analysis considers a zero-mean noise which gets attenuated in the HR image reconstruction by fusing many images. The resulting probabilistic upper bounds are a good complement to the Cramer-Rao lower bounds in [11] and are nearly tight since the order of magnitudes are similar. Numerical experiments illustrate our results in both the Fourier and spatial domains as well as the effect of the PSF. A strong aspect of this work is in its predictions for practical implementation. Such results also give precious hints on the design of SR systems. Future works may investigate similar probabilistic bounds for more sophisticated SR algorithms where some reconstruction priors are used [25]–[28].

Fig. 8. (l.) Barbara, (r.) contribution of the less reliable frequencies.

## Appendix

### A. Proofs of Lemma 1 & 2

*Proof of Lemma 1:* $\sqrt{x_1^2 + x_2^2} \geq \sqrt{a_1^2 + a_2^2} \Rightarrow |x_1| \geq a_1$ or $|x_2| \geq a_2$ proves (17), see figure 9(a). $|x_1| + |x_2| \geq a_1 + a_2 \Rightarrow |x_1| \geq a_1$ or $|x_2| \geq a_2$ proves (18), see fig. 9(b) where the grey lozenge represents the region $|x_1| + |x_2| \leq a_1 + a_2$.
*Proof of Lemma 2:* $\forall i,\ |x_i| \leq a_i \Rightarrow \sum_i |x_i| \leq \sum_i a_i$ so that $P\left(\sum_i |x_i| \leq \sum a_i\right) \geq P\left(\{\forall i,\ |x_i| \leq a_i\}\right)$. Since the $x_i$ are independent, $P\left(\{\forall i,\ |x_i| \leq a_i\}\right) = \prod_i P(|x_i| \leq a_i)$. Noting that $\forall i,\ P(|x_i| \leq a_i) \geq (1 - P_i)$ concludes the proof. *QED.*

### B. Proof of concentration inequality (20)

As far as the real part of $B_G$ in (16) is concerned:

$$\mathcal{R}e\left(B_G\right) = \frac{1}{r^2 n_{\mathbf{d}}} \sum_{\mathbf{d},j} \cos\left(\mathbf{q}_{\boldsymbol{\gamma}}.\mathbf{b}_{\mathbf{d}j}\right) - \mathbb{E}[\cos\left(\mathbf{q}_{\boldsymbol{\gamma}}.\mathbf{b}_{\mathbf{d}j}\right)] \quad (65)$$

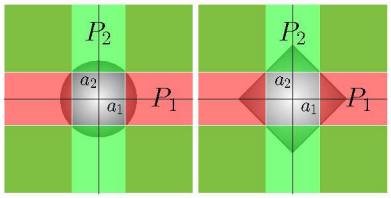


(a) (b)

Fig. 9. Illustrations for the proof of Lemma 1.

The power series development of the cos function yields:

$$\left|\cos(\mathbf{q}_{\boldsymbol{\gamma}}\cdot\mathbf{b}_{\mathbf{d}j})-1+\frac{(\mathbf{q}_{\boldsymbol{\gamma}}\cdot\mathbf{b}_{\mathbf{d}j})^2}{2}\right|\leq\frac{\|\mathbf{q}_{\boldsymbol{\gamma}}\|_1^4\epsilon_r^4}{24} \quad (66)$$

so that

$$|\mathcal{R}e\,(B_G)|\leq\left|\frac{1}{2r^2n_{\mathbf{d}}}\sum_{\mathbf{d},j}(\mathbf{q}_{\boldsymbol{\gamma}}.\mathbf{b}_{\mathbf{d}j})^2-\mathbb{E}[(\mathbf{q}_{\boldsymbol{\gamma}}.\mathbf{b}_{\mathbf{d}j})^2]\right|+\frac{\|\mathbf{q}_{\boldsymbol{\gamma}}\|_1^4\epsilon_r^4}{12} \quad (67)$$

The first term is the sum of bounded centered random variables since $(\mathbf{q}_{\boldsymbol{\gamma}}.\mathbf{b}_{\mathbf{d}j})^2$ and $\mathbb{E}[(\mathbf{q}_{\boldsymbol{\gamma}}.\mathbf{b}_{\mathbf{d}j})^2]$ belong to $(0,\|\mathbf{q}_{\boldsymbol{\gamma}}\|_1^2\,\epsilon_r^2)$. Applying Hoeffding's inequality for random variables in $(-\|\mathbf{q}_{\boldsymbol{\gamma}}\|_1^2\,\epsilon_r^2,\|\mathbf{q}_{\boldsymbol{\gamma}}\|_1^2\,\epsilon_r^2)$ and $t=\delta_{\boldsymbol{\gamma}}=c(\mathbf{q}_{\boldsymbol{\gamma}})\|\mathbf{q}_{\boldsymbol{\gamma}}\|_1\epsilon$ yields:

$$P\left(|\mathcal{R}e\,(B_G)|\geq\delta_{\boldsymbol{\gamma}}+\frac{\|\mathbf{q}_{\boldsymbol{\gamma}}\|_1^4\epsilon_r^4}{12}\right)\leq 2e^{-\frac{c^2n_{\mathbf{d}}}{2\|\mathbf{q}_{\boldsymbol{\gamma}}\|_1^2\epsilon_r^2}} \quad (68)$$

since $\sum_{\mathbf{d},j}$ involves $r^2n_{\mathbf{d}}$ terms and $\epsilon_r=\epsilon r$. Turning to the imaginary part, the same kind of arguments are applied to

$$\mathcal{I}m\,(B_G)=\frac{1}{r^2n_{\mathbf{d}}}\sum_{\mathbf{d},j}\sin\,(\mathbf{q}_{\boldsymbol{\gamma}}.\mathbf{b}_{\mathbf{d}j})-\mathbb{E}[\sin\,(\mathbf{q}_{\boldsymbol{\gamma}}.\mathbf{b}_{\mathbf{d}j})] \quad (69)$$

to show that

$$|\mathcal{I}m\,(B_G)|\leq\left|\frac{1}{r^2n_{\mathbf{d}}}\sum_{\mathbf{d},j}(\mathbf{q}_{\boldsymbol{\gamma}}\cdot\mathbf{b}_{\mathbf{d}j}-\mathbb{E}[\mathbf{q}_{\boldsymbol{\gamma}}\cdot\mathbf{b}_{\mathbf{d}j}])\right|+\frac{\|\mathbf{q}_{\boldsymbol{\gamma}}\|_1^3\epsilon_r^3}{3} \quad (70)$$

We prove a concentration inequality similar to (68) by applying Hoeffding's inequality to the first term of (70) since $|\mathbf{q}\cdot\mathbf{b}-\mathbb{E}[\mathbf{q}\cdot\mathbf{b}]|\leq 2\|\mathbf{q}\|_1\,\epsilon_r$. For $\delta_{\boldsymbol{\gamma}}=c(\mathbf{q}_{\boldsymbol{\gamma}})\|\mathbf{q}_{\boldsymbol{\gamma}}\|_1\epsilon>0$,

$$P\left(|\mathcal{I}m\,(B_G)|\geq\delta_{\boldsymbol{\gamma}}+\frac{\|\mathbf{q}_{\boldsymbol{\gamma}}\|_1^3\epsilon_r^3}{3}\right)\leq 2e^{-c^2n_{\mathbf{d}}/8} \quad (71)$$

Using Lemma 1 to combine (68) and (71) yields:

$$P\left(|B_G|\geq\sqrt{\left(\delta_{\boldsymbol{\gamma}}+\frac{\|\mathbf{q}_{\boldsymbol{\gamma}}\|_1^4\epsilon_r^4}{12}\right)^2+\left(\delta_{\boldsymbol{\gamma}}+\frac{\|\mathbf{q}_{\boldsymbol{\gamma}}\|_1^3\epsilon_r^3}{3}\right)^2}\right)\leq 2\left(e^{-c^2n_{\mathbf{d}}/8}+e^{-\frac{c^2n_{\mathbf{d}}}{2\|\mathbf{q}_{\boldsymbol{\gamma}}\|_1^2\epsilon_r^2}}\right) \quad (72)$$

Note that $\frac{\|\mathbf{q}_{\boldsymbol{\gamma}}\|_1^4\epsilon_r^4}{12}\leq\frac{\|\mathbf{q}_{\boldsymbol{\gamma}}\|_1^3\epsilon_r^3}{3}$ as soon as $\epsilon_r\leq 4/\pi$. Remark that $2\|\mathbf{q}_{\boldsymbol{\gamma}}\|_1^2\epsilon^2\leq 8\pi^2\epsilon_r^2<8$ for $\epsilon<1/\pi r$. This yields (20).

### C. Proof of concentration inequalities (30) & (31)

First, we deal with the real part of $G_{\boldsymbol{\alpha}}(\mathbf{k}')$in (28):

$$\mathcal{R}e\,(G_{\boldsymbol{\alpha}}(\mathbf{k}'))=\frac{1}{r^2n_{\mathbf{d}}}\sum_{\mathbf{d},j}\cos\,(\theta_{\boldsymbol{\alpha}\mathbf{d}}-\mathbf{q}_{\boldsymbol{\alpha}}\cdot\mathbf{b}_{\mathbf{d}j}) \quad (73)$$

The power series development of cosinus around $\theta_{\boldsymbol{\alpha}\mathbf{d}}$ yields:

$$\begin{aligned}\cos(\theta_{\boldsymbol{\alpha}\mathbf{d}}-\mathbf{q}_{\boldsymbol{\alpha}}\cdot\mathbf{b}_{\mathbf{d}j})-\cos\,(\theta_{\boldsymbol{\alpha}\mathbf{d}})-\sin\,(\theta_{\boldsymbol{\alpha}\mathbf{d}})\,(\mathbf{q}_{\boldsymbol{\alpha}}\cdot\mathbf{b}_{\mathbf{d}j})=\\ \cos(\theta_{\boldsymbol{\alpha}\mathbf{d}})\sum_{k=1}^{\infty}(-1)^k\frac{(\mathbf{q}_{\boldsymbol{\alpha}}\cdot\mathbf{b}_{\mathbf{d}j})^{2k}}{(2k)!}\\ +\sin(\theta_{\boldsymbol{\alpha}\mathbf{d}})\sum_{k=1}^{\infty}(-1)^k\frac{(\mathbf{q}_{\boldsymbol{\alpha}}\cdot\mathbf{b}_{\mathbf{d}j})^{2k+1}}{(2k+1)!}\end{aligned} \quad (74)$$

The majorization of the rest of alternating power series yields:

$$\begin{aligned}|\cos(\theta_{\boldsymbol{\alpha}\mathbf{d}}-\mathbf{q}_{\boldsymbol{\alpha}}.\mathbf{b}_{\mathbf{d}j})-\cos\theta_{\boldsymbol{\alpha}\mathbf{d}}-(\mathbf{q}_{\boldsymbol{\alpha}}.\mathbf{b}_{\mathbf{d}j})\sin\theta_{\boldsymbol{\alpha}\mathbf{d}}|\\ \leq|\cos\theta_{\boldsymbol{\alpha}\mathbf{d}}|\frac{|\mathbf{q}_{\boldsymbol{\alpha}}\cdot\mathbf{b}_{\mathbf{d}j}|^2}{2}+|\sin\theta_{\boldsymbol{\alpha}\mathbf{d}}|\frac{|\mathbf{q}_{\boldsymbol{\alpha}}\cdot\mathbf{b}_{\mathbf{d}j}|^3}{6}\end{aligned} \quad (75)$$

As a consequence,

$$\begin{aligned}\mathcal{R}e\,(G_{\boldsymbol{\alpha}}(\mathbf{k}'))\leq f(\mathbf{q}_{\boldsymbol{\alpha}},\epsilon_r)\\ +\left|\frac{1}{r^2n_{\mathbf{d}}}\sum_{\mathbf{d},j}\cos\theta_{\boldsymbol{\alpha}\mathbf{d}}+(\mathbf{q}_{\boldsymbol{\alpha}}\cdot\mathbf{b}_{\mathbf{d}j})\sin\theta_{\boldsymbol{\alpha}\mathbf{d}}\right|\end{aligned} \quad (76)$$

where

$$f(\mathbf{q}_{\boldsymbol{\alpha}},\epsilon_r)=\frac{\|\mathbf{q}_{\boldsymbol{\alpha}}\|_1^2\epsilon_r^2}{2}+\frac{\|\mathbf{q}_{\boldsymbol{\alpha}}\|_1^3\epsilon_r^3}{6} \quad (77)$$

Thanks to (95) in Appendix E,

$$\mathcal{R}e\,(G_{\boldsymbol{\alpha}})\leq\left|\frac{1}{r^2n_{\mathbf{d}}}\sum_{\mathbf{d},j}(\mathbf{q}_{\boldsymbol{\alpha}}\cdot\mathbf{b}_{\mathbf{d}j})\sin\theta_{\boldsymbol{\alpha}\mathbf{d}}\right|+f(\mathbf{q}_{\boldsymbol{\alpha}},\epsilon_r) \quad (78)$$

For $\boldsymbol{\alpha}-\boldsymbol{\gamma}\in\{0,r/2\}^2$, $\theta_{\boldsymbol{\alpha}\mathbf{d}}\propto\pi\Rightarrow\sin\theta_{\boldsymbol{\alpha}\mathbf{d}}=0$ for all $\mathbf{d}$ and (75) yields the deterministic tight inequality

$$\mathcal{R}e\,(G_{\boldsymbol{\alpha}}(\mathbf{k}'))\leq\frac{\|\mathbf{q}_{\boldsymbol{\alpha}}\|_1^2\epsilon_r^2}{2} \quad (79)$$

Turning to the imaginary part, we follow the same lines by mainly replacing 'cos' by 'sin' in (76) & (78) starting from

$$\begin{aligned}|\sin(\theta_{\boldsymbol{\alpha}\mathbf{d}}-\mathbf{q}_{\boldsymbol{\alpha}}.\mathbf{b}_{\mathbf{d}j})-\sin\theta_{\boldsymbol{\alpha}\mathbf{d}}+(\mathbf{q}_{\boldsymbol{\alpha}}.\mathbf{b}_{\mathbf{d}j})\cos\theta_{\boldsymbol{\alpha}\mathbf{d}}|\\ \leq|\sin\theta_{\boldsymbol{\alpha}\mathbf{d}}|\frac{|\mathbf{q}_{\boldsymbol{\alpha}}.\mathbf{b}_{\mathbf{d}j}|^2}{2}+|\cos\theta_{\boldsymbol{\alpha}\mathbf{d}}|\frac{|\mathbf{q}_{\boldsymbol{\alpha}}.\mathbf{b}_{\mathbf{d}j}|^3}{6}\end{aligned} \quad (80)$$

to obtain the following bound on the imaginary part:

$$|\mathcal{I}m\,(G_{\boldsymbol{\alpha}})|\leq\left|\frac{1}{r^2n_{\mathbf{d}}}\sum_{\mathbf{d},j}(\mathbf{q}_{\boldsymbol{\alpha}}.\mathbf{b}_{\mathbf{d}j})\cos\theta_{\boldsymbol{\alpha}\mathbf{d}}\right|+f(\mathbf{q}_{\boldsymbol{\alpha}},\epsilon_r) \quad (81)$$

Then one needs to bound the sums in the r.h.s. of (78) & (81). Assuming that the variations of the bias $\mathbb{E}[\mathbf{q}_{\boldsymbol{\alpha}}\cdot\mathbf{b}_{\mathbf{d}j}]$ around $\langle\mathbb{E}[\mathbf{q}_{\boldsymbol{\alpha}}\cdot\mathbf{b}_{\mathbf{d}j}]\rangle_{\mathbf{d}}$ for fixed $\mathbf{d}$ are negligible, one observes that there is (approximately) no contribution of the bias in the sums of (78) & (81) thanks to (95) & (96). Indeed,

$$\frac{1}{r^2n_{\mathbf{d}}}\sum_{\mathbf{d},j}\cos(\theta_{\boldsymbol{\alpha}\mathbf{d}})\langle\mathbb{E}[\mathbf{q}_{\boldsymbol{\alpha}}.\mathbf{b}_{\mathbf{d}j}]\rangle_{\mathbf{d}})\simeq 0 \quad (82)$$

Since $|\mathbf{q}_{\boldsymbol{\alpha}} \cdot \mathbf{b}_{\mathbf{d}j}| \leq \|\mathbf{q}_{\boldsymbol{\alpha}}\|_1 \epsilon_r$, we apply Hoeffding's inequality to (78) and (81) for $\delta_{\boldsymbol{\alpha}} = c\|\mathbf{q}_{\boldsymbol{\alpha}}\|_1\epsilon$, and for $\boldsymbol{\alpha}-\boldsymbol{\gamma} \notin \{0, r/2\}^2$:

$$P\left(|\mathcal{R}e\left(G_{\boldsymbol{\alpha}}(\mathbf{k}')\right)| \geq \delta'_{\boldsymbol{\alpha}}\right) \leq 2e^{-\frac{2r^2 n_{\mathbf{d}}^2 c^2}{4\sum_{\mathbf{d},j} \sin^2 \theta_{\boldsymbol{\alpha}\mathbf{d}}}} \tag{83}$$

$$P\left(|\mathcal{I}m\left(G_{\boldsymbol{\alpha}}(\mathbf{k}')\right)| \geq \delta'_{\boldsymbol{\alpha}}\right) \leq 2e^{-\frac{2r^2 n_{\mathbf{d}}^2 c^2}{4\sum_{\mathbf{d},j} \cos^2 \theta_{\boldsymbol{\alpha}\mathbf{d}}}} \tag{84}$$

where $\delta'_{\boldsymbol{\alpha}} = c\|\mathbf{q}_{\boldsymbol{\alpha}}\|_1\epsilon + f(\mathbf{q}_{\boldsymbol{\alpha}}, \epsilon_r)$. Using (97) & (98) in App. E, Lemma 1 yields inequalities (30) & (31).

### D. Computing $c_2(p)$ in (36)

Here we estimate $c_2(p)$ in (36) under assumptions of Theorem 3. If one neglects the effect of blur, we aim at computing the maximum value of $c_2(p)$ such that for all $\mathbf{q}_{\boldsymbol{\gamma}}$,

$$a\, c_2(p) + p_0 \leq p. \tag{85}$$

after little reorganization of (34) where we use

$$p_0 \simeq \frac{\sqrt{2}}{2} \sum_{\boldsymbol{\alpha}\neq\boldsymbol{\gamma}} \frac{|Y(\mathbf{q}_{\boldsymbol{\alpha}})|}{|Y(\mathbf{q}_{\boldsymbol{\gamma}})|} \|\mathbf{q}_{\boldsymbol{\alpha}}\|_1^2 \epsilon_r^2 \tag{86}$$

$$a = \sqrt{2} \sum_{\boldsymbol{\alpha}\neq\boldsymbol{\gamma}} \frac{|Y(\mathbf{q}_{\boldsymbol{\alpha}})|}{|Y(\mathbf{q}_{\boldsymbol{\gamma}})|} \|\mathbf{q}_{\boldsymbol{\alpha}}\|_1 \epsilon. \tag{87}$$

as soon as $\epsilon_r \ll 1$ so that cubic terms can be neglected. We first study (86). We focus on the highest frequencies only, typically $\mathbf{q}_{\boldsymbol{\gamma}} = (\pi - \frac{2\pi}{rN}, \pi - \frac{2\pi}{rN})$. As a consequence, note that $\|\mathbf{q}_{\boldsymbol{\gamma}}\|_2^{1+\eta} \simeq (\sqrt{2}\pi)^{1+\eta}$. Then, one needs to detail:

$$\sum_{\boldsymbol{\alpha}\neq\boldsymbol{\gamma}} \frac{\|\mathbf{q}_{\boldsymbol{\alpha}}\|_1^2}{\|\mathbf{q}_{\boldsymbol{\alpha}}\|_2^{1+\eta}} = \frac{\pi^2}{\pi^{1+\eta}} \underbrace{\sum_{\boldsymbol{\beta}\neq(0,0)} \frac{\|\mathbf{v}_{rN} - 2\boldsymbol{\beta}/r\|_1^2}{\|\mathbf{v}_{rN} - 2\boldsymbol{\beta}/r\|_2^{1+\eta}}}_{F(r,N)} \tag{88}$$

where $\mathbf{v}_{rN} = (1 - 2/rN, 1 - 2/rN)$. The sum $F(r, N)$ can be computed numerically. It weakly depends on $N$ so that

$$F(r,N) \simeq \begin{cases} 2 = \dfrac{2}{3}(r^2-1) & \text{if } r = 2, \\ 1.2(r^2-1) & \text{if } r \geq 3. \end{cases} \tag{89}$$

For $r = 2$, computations are easy and only 2 terms both equal to 1 appear in $F(r, N)$. For $r \geq 3$, one can observe that $\|\mathbf{q}_{\boldsymbol{\alpha}}\|_1 \sim \|\mathbf{q}_{\boldsymbol{\alpha}}\|_2$ (norms are equivalent) so that when $\eta = 0$ one expects that $F(r, N) \propto (r^2 - 1)$, the number of terms in $\sum_{\boldsymbol{\beta}\neq(0,0)}$. This is due to the fact that $\langle \|\mathbf{q}_{\boldsymbol{\alpha}}\|_1 \rangle_{\boldsymbol{\alpha}\neq\boldsymbol{\gamma}} \simeq \pi$ for large $r$. As a result, one obtains in good approximation that :

$$p_0 \simeq b_0 \sqrt{2}^{\eta} \pi^2 \epsilon^2 r^2 (r^2 - 1) \tag{90}$$

where $b_0 = 2/3$ if $r = 2$ or $b_0 \simeq 1.2$ if $r \geq 3$. Now let study coefficient (87) along the same lines.

$$a \simeq \sqrt{2} \sum_{\boldsymbol{\alpha}\neq\boldsymbol{\gamma}} \frac{\|\mathbf{q}_{\boldsymbol{\gamma}}\|_2^{1+\eta}}{\|\mathbf{q}_{\boldsymbol{\alpha}}\|_2^{1+\eta}} \|\mathbf{q}_{\boldsymbol{\alpha}}\|_1 \epsilon \tag{91}$$

Using that $\|\mathbf{q}_{\boldsymbol{\alpha}}\|_1 \sim \|\mathbf{q}_{\boldsymbol{\alpha}}\|_2$ (within constant factors), one expects that when $\eta = 0$,

$$a \propto 2^{1+\eta/2}(r^2 - 1)\epsilon \tag{92}$$

Numerical estimates for values $2 \leq r \leq 8$ show that

$$a = a_0 \times 2^{1+\eta/2}\epsilon(r^2 - 1) \tag{93}$$

where $a_0$ varies with $\eta$ around a typical value of 1.3 for $\eta = 0$, e.g. $a_0 \simeq 0.95$ if $\eta = -0.2$ and $a_0 \simeq 1.85$ if $\eta = 0.2$ for all $r \geq 3$. For $r = 2$, one finds $a_0 \simeq 0.63$, resp. 1.14 and 3.04 when $\eta = -0.2$, resp. 0 and 0.2.

### E. Properties of complex roots of unity

$$\theta_{\boldsymbol{\alpha}\mathbf{d}} = \frac{2\pi}{r}(\boldsymbol{\alpha} - \boldsymbol{\gamma})\mathbf{d} = \frac{2\pi}{r}\boldsymbol{\delta}\mathbf{d} \tag{94}$$

where $\boldsymbol{\alpha}$ and $\boldsymbol{\gamma}$ are integers in $(0, r-1)^2$. The set of the $\theta_{\boldsymbol{\alpha}\mathbf{d}}$ matches the set of products of complex roots of unity so that:

$$\sum_{\mathbf{d}} \cos\left(\frac{2\pi}{r}(\boldsymbol{\alpha} - \boldsymbol{\gamma})\mathbf{d}\right) = \sum_{\mathbf{d}} \cos(\theta_{\boldsymbol{\alpha}\mathbf{d}}) = 0 \tag{95}$$

$$\sum_{\mathbf{d}} \sin\left(\frac{2\pi}{r}(\boldsymbol{\alpha} - \boldsymbol{\gamma})\mathbf{d}\right) = \sum_{\mathbf{d}} \sin(\theta_{\boldsymbol{\alpha}\mathbf{d}}) = 0 \tag{96}$$

$$\sum_{\mathbf{d}} \cos^2(\theta_{\boldsymbol{\alpha}\mathbf{d}}) = \begin{cases} r^2 \text{ if } \boldsymbol{\alpha} - \boldsymbol{\gamma} \in \{0, r/2\}^2, \\ r/2 \text{ otherwise.} \end{cases} \tag{97}$$

$$\sum_{\mathbf{d}} \sin^2(\theta_{\boldsymbol{\alpha}\mathbf{d}}) = \begin{cases} 0 \text{ if } \boldsymbol{\alpha} - \boldsymbol{\gamma} \in \{0, r/2\}^2, \\ r/2 \text{ otherwise.} \end{cases} \tag{98}$$

Properties (95) and (96) come from the observation that

$$\sum_{\mathbf{d}\in(0,r-1)^2} e^{i\theta_{\boldsymbol{\alpha}\mathbf{d}}} = \prod_{i=1,2} \left( \sum_{d_i \in (0,r-1)} e^{i2\pi(\alpha_i - \gamma_i)d_i/r} \right) \tag{99}$$

where each factor in the r.h.s. is zero since $\boldsymbol{\alpha} \neq \boldsymbol{\gamma}$ and for any integer $1 \leq \delta \leq r-1$,

$$\sum_{d=0}^{r-1} e^{i2\pi\delta d/r} = \frac{1 - e^{i2\pi\delta}}{1 - e^{i2\pi\delta/r}} = 0 \tag{100}$$

Now we prove (97) and (98). To this aim we need:

$$\cos^2(\theta_{\boldsymbol{\alpha}\mathbf{d}}) = \frac{1 + \cos(2\theta_{\boldsymbol{\alpha}\mathbf{d}})}{2} \tag{101}$$

$$\sin^2(\theta_{\boldsymbol{\alpha}\mathbf{d}}) = \frac{1 - \cos(2\theta_{\boldsymbol{\alpha}\mathbf{d}})}{2} \tag{102}$$

We need to evaluate $\sum_{d=0}^{r-1} e^{i2\theta_{\boldsymbol{\alpha}\mathbf{d}}}$. For $0 \leq \delta \leq r-1$,

$$\sum_{d=0}^{r-1} e^{i4\pi\delta d/r} = \begin{cases} \sum_{d=0}^{r-1} 1 = r & \text{if } \delta \in \{0, r/2\}, \\ \dfrac{1 - e^{i4\pi\delta}}{1 - e^{i4\pi\delta/r}} = 0 & \text{otherwise,} \end{cases} \tag{103}$$

so that using (99) again

$$\sum_{\mathbf{d}} e^{i2\theta_{\boldsymbol{\alpha}\mathbf{d}}} = \begin{cases} r^2 \text{ if } \boldsymbol{\alpha} - \boldsymbol{\gamma} \in \{0, r/2\}^2, \\ 0 \text{ otherwise.} \end{cases} \tag{104}$$

Taking the real part yields $\sum_{\mathbf{d}} \cos(2\theta_{\boldsymbol{\alpha}\mathbf{d}})$. The sum of (101) & (102) over $\mathbf{d} \in (0, r-1)^2$ yield (97) & (98).

### F. Expectations $\mathbb{E}[G_{\boldsymbol{\alpha}}]$

Taking the expectation of (13) with respect to $\mathbf{b}_{\mathbf{d}j}$ yields:

$$\mathbb{E}G_{\boldsymbol{\alpha}}(\mathbf{k}') = \sum_{\mathbf{d}} e^{-i\frac{2\pi}{r}(\boldsymbol{\alpha}-\boldsymbol{\gamma})\cdot\mathbf{d}} \mathbb{E}\left[e^{-i\frac{2\pi}{rN}\mathbf{k}'_{\boldsymbol{\alpha}}\cdot\mathbf{b}_{\mathbf{d}j}}\right] \tag{105}$$

Then let $\chi(\mathbf{k}') = \mathbb{E}\left[e^{-i\frac{2\pi}{rN}\mathbf{k}'\cdot\mathbf{b}_{\mathbf{d}j}}\right]$ the characteristic function of the distribution of $\mathbf{b}_{\mathbf{d}j}$. It results from properties of roots of unity above that

$$\sum_{\mathbf{d}} e^{-i\frac{2\pi}{r}(\boldsymbol{\alpha}-\boldsymbol{\gamma})\mathbf{d}} = \begin{cases} 0 \text{ when } \boldsymbol{\alpha} \neq \boldsymbol{\gamma}, \\ r^2 \text{ when } \boldsymbol{\alpha} = \boldsymbol{\gamma} \end{cases} \tag{106}$$

so that denoting Kronecker's symbol by $\delta_{\boldsymbol{\gamma}\boldsymbol{\alpha}}$:

$$\mathbb{E}G_{\boldsymbol{\alpha}}(\mathbf{k}') = \delta_{\boldsymbol{\gamma}\boldsymbol{\alpha}}\, \chi(\mathbf{k}') \tag{107}$$

### *G. The $G_{\boldsymbol{\alpha}}$ are uncorrelated*

The correlation between $G_{\boldsymbol{\alpha}_1}$ and $G_{\boldsymbol{\alpha}_2}$ for $\boldsymbol{\alpha}_i \neq \boldsymbol{\gamma}$ is:

$$\begin{aligned}\mathbb{E}[G_{\boldsymbol{\alpha}_1} G^*_{\boldsymbol{\alpha}_2}] = \frac{1}{n_{\mathbf{d}}^2} \sum_{\mathbf{d}\mathbf{d}'} e^{-i\frac{2\pi}{rN}(\boldsymbol{\alpha}_1-\boldsymbol{\gamma})\mathbf{d}N} e^{+i\frac{2\pi}{rN}(\boldsymbol{\alpha}_2-\boldsymbol{\gamma})\mathbf{d}'N} \\ \times \sum_{j,\ell=1}^{n_{\mathbf{d}}} \underbrace{\mathbb{E}\left[e^{+i\frac{2\pi}{rN}(\mathbf{k}'+\boldsymbol{\alpha}_1 N)\cdot\mathbf{b}_{\mathbf{d}j}} e^{-i\frac{2\pi}{rN}(\mathbf{k}'+\boldsymbol{\alpha}_2 N)\cdot\mathbf{b}_{\mathbf{d}\ell}}\right]}_{\beta_{j\ell}}\end{aligned}$$

One remarks that

$$\beta_{j\ell} = \begin{cases} \chi((\boldsymbol{\alpha}_2-\boldsymbol{\alpha}_1)N) & \text{if } j=\ell, \\ \chi(\mathbf{k}'_{\boldsymbol{\alpha}_1})\chi(-\mathbf{k}'_{\boldsymbol{\alpha}_2}) & \text{if } j\neq\ell, \end{cases} \tag{108}$$

so that

$$\begin{aligned}\mathbb{E}[G_{\boldsymbol{\alpha}_1}(\mathbf{k}')G^*_{\boldsymbol{\alpha}_2}(\mathbf{k}')] = \frac{1}{n_{\mathbf{d}}^2}\left(\sum_{\mathbf{d}} e^{-i\frac{2\pi}{rN}(\boldsymbol{\alpha}_1-\boldsymbol{\alpha}_2)\mathbf{d}N}\right) \\ \times \left(\sum_{j,\ell=1}^{n_{\mathbf{d}}} \beta_{j\ell} - \sum_{j,\ell=1}^{n_{\mathbf{d}}} \chi(\mathbf{k}'_{\boldsymbol{\alpha}_1})\chi(-\mathbf{k}'_{\boldsymbol{\alpha}_2})\right)\end{aligned} \tag{109}$$

Then using (108) and little algebra one gets

$$\begin{aligned}\sum_{j,\ell=1}^{n_{\mathbf{d}}} \beta_{j\ell} - \sum_{j,\ell=1}^{n_{\mathbf{d}}} \chi(\mathbf{k}'_{\boldsymbol{\alpha}_1})\chi(-\mathbf{k}'_{\boldsymbol{\alpha}_2}) \\ = n_{\mathbf{d}}\left[\chi((\boldsymbol{\alpha}_2-\boldsymbol{\alpha}_1)N) - \chi(\mathbf{k}'_{\boldsymbol{\alpha}_1})\chi(-\mathbf{k}'_{\boldsymbol{\alpha}_2})\right]\end{aligned} \tag{110}$$

As a consequence one finally gets:

$$\begin{aligned}\mathbb{E}[G_{\boldsymbol{\alpha}_1}(\mathbf{k}')G^*_{\boldsymbol{\alpha}_2}(\mathbf{k}')] \\ = \delta_{\boldsymbol{\alpha}_1\boldsymbol{\alpha}_2}\frac{r^2}{n_{\mathbf{d}}}\left[\chi((\boldsymbol{\alpha}_2-\boldsymbol{\alpha}_1)N) - \chi(\mathbf{k}'_{\boldsymbol{\alpha}_1})\chi(-\mathbf{k}'_{\boldsymbol{\alpha}_2})\right] \\ = \delta_{\boldsymbol{\alpha}_1\boldsymbol{\alpha}_2}\frac{r^2}{n_{\mathbf{d}}}\left(1-|\chi(\mathbf{k}'_{\boldsymbol{\alpha}_1})|^2\right)\end{aligned} \tag{111}$$

so that the $G_{\boldsymbol{\alpha}_i}$, $\boldsymbol{\alpha}_i \neq \boldsymbol{\gamma}$, are uncorrelated. QED.

## REFERENCES


[1] M. Elad and Y. Hel-Or, "A fast super-resolution reconstruction algorithm for pure translational motion and common space-invariant blur," *IEEE Trans. Image Process.*, vol. 10, no. 8, pp. 1187–1193, 2001.

[2] C. Yamahata, E. Sarajlic, G. J. M. Krijnen, and M. A. M. Gijs, "Subnanometer translation of microelectromechanical systems measured by discrete fourier analysis of ccd images," *Microelectromechanical Systems, Journal of*, vol. 19, no. 5, pp. 1273–1275, 2010.

[3] M. Protter, M. Elad, H. Takeda, and P. Milanfar, "Generalizing the nonlocal-means to super-resolution reconstruction," *IEEE Trans. Image Process.*, vol. 18, no. 1, pp. 36–51, 2009.

[4] J. Yang and T. Huang, *Super resolution imaging*, ch. Image super-resolution: historical overview and future challenges. CRC Press, 2011.

[5] M. Ng and N. Bose, "Analysis of displacement errors in high-resolution image reconstruction with multisensors," *IEEE Trans. Circuits-Syst. I: Fundam. Theory*, vol. 49, no. 6, pp. 806–813, 2002.

[6] M. Ng and N. Bose, "Mathematical analysis of super-resolution methodology," *IEEE Signal Process. Mag.*, vol. 20, no. 3, pp. 62–74, 2003.

[7] N. Bose, H. C. Kim, and B. Zhou, "Performance analysis of the tls algorithm for image reconstruction from a sequence of undersampled noisy and blurred frames," in *Proc. of IEEE International Conference on Image Processing*, vol. 3, pp. 571–574 vol.3, Nov 1994.

[8] S. Baker and T. Kanade, "Limits on super-resolution and how to break them," *IEEE Trans. Pattern Anal. Mach. Intell.*, vol. 24, no. 9, pp. 1167–1183, 2002.

[9] Y. Traonmilin, S. Ladjal, and A. Almansa, "On the Amount of Regularization for Super-Resolution Interpolation," in *20th European Signal Processing Conference 2012 (EUSIPCO 2012)*, (Roumanie), pp. 380 – 384, Aug. 2012.

[10] F. Champagnat, G. L. Besnerais, and C. Kulcsár, "Statistical performance modeling for superresolution: a discrete data-continuous reconstruction framework," *J. Opt. Soc. Am. A*, vol. 26, pp. 1730–1746, Jul 2009.

[11] D. Robinson and P. Milanfar, "Statistical performance analysis of super-resolution," *IEEE Trans. Image Process.*, vol. 15, no. 6, pp. 1413–1428, 2006.

[12] R. Tsai and T. Huang, "Multiframe image restoration and registration," in *Advances in Computer Vision and Image Processing* (R. Tsai and T. Huang, eds.), vol. 1, pp. 317–339, JAI Press Inc., 1984.

[13] Z. Lin and H.-Y. Shum, "Fundamental limits of reconstruction-based superresolution algorithms under local translation," *IEEE Trans. Pattern Anal. Mach. Intell.*, vol. 26, no. 1, pp. 83–97, 2004.

[14] P. Chainais, A. Leray, and P. Pfennig, "Quantitative control of the error bounds of a fast super-resolution technique for microscopy and astronomy," in *Proc. of ICASSP*, 2014.

[15] S. Farsiu, D. Robinson, M. Elad, and P. Milanfar, "Advances and challenges in super-resolution," *International Journal of Imaging Systems and Technology*, vol. 14, no. 2, pp. 47–57, 2004.

[16] A. Bovik, *The Essential Guide to Image Processing*. Academic Press, 2009.

[17] H. Foroosh, J. Zerubia, and M. Berthod, "Extension of phase correlation to subpixel registration," *IEEE Trans. Image Process.*, vol. 11, no. 3, pp. 188–200, 2002.

[18] D. Robinson, S. Farsiu, and P. Milanfar, "Optimal registration of aliased images using variable projection with applications to super-resolution," *The Computer Journal*, vol. 52, no. 1, pp. 31–42, 2007.

[19] M. Ben-Ezra, A. Zomet, and S. Nayar, "Video super-resolution using controlled subpixel detector shifts," *Pattern Analysis and Machine Intelligence, IEEE Transactions on*, vol. 27, pp. 977–987, June 2005.

[20] W. Feller, *An Introduction to Probability Theory and Its Applications*, vol. 2. New-York, London, Sidney: John Wiley and Sons, Inc., 1966.

[21] S. Boucheron, G. Lugosi, and P. Massart, *Concentration inequalities*. Oxford University Press, 2013.

[22] D. Mumford and B. Gidas, "Stochastic models for generic images," *Quarterly of applied mathematics*, vol. LIV, no. 1, pp. 85–111, 2001.

[23] D. Ruderman and W. Bialek, "Statistics of natural images: scaling in the woods," *Physical Review Letters*, vol. 73, no. 3, pp. 814–817, 1994.

[24] P. Chainais, "Infinitely divisible cascades to model the statistics of natural images," *IEEE Trans. on Patt. and Mach. Intell.*, vol. 29, no. 12, pp. 2105–2118, 2007.

[25] S. Farsiu, M. Robinson, M. Elad, and P. Milanfar, "Fast and robust multiframe super resolution," *IEEE Trans. Image Process.*, vol. 13, no. 10, pp. 1327–1344, 2004.

[26] R. Hardie, "A fast image super-resolution algorithm using an adaptive wiener filter," *IEEE Trans. Image Process.*, vol. 16, no. 12, pp. 2953–2964, 2007.

[27] P. Vandewalle, L. Sbaiz, J. Vandewalle, and M. Vetterli, "Super-resolution from unregistered and totally aliased signals using subspace methods," *IEEE Trans. Signal Process.*, vol. 55, no. 7, part 2, pp. 3687–3703, 2007.

[28] J. Yang, J. Wright, T. Huang, and Y. Ma, "Image super-resolution via sparse representation," *IEEE Trans. on Image Process.*, vol. 19, pp. 2861–2873, Nov 2010.